A Satellite Study of VLF Emissions During Magnetic Storms*

by

David P. Cauffman

A thesis submitted in partial fulfillment of the
requirements for the degree of Master of Science
in the Department of Physics and Astronomy
in the Graduate College of
The University of Iowa

June, 1968

Thesis supervisor: Assistant Professor Donald A. Gurnett

*Supported in part by the National Aeronautics and Space Administration under Contract No. NGR-16-001-043 and the Office of Naval Research under Contract No. Nonr 1509(06).

Certificate of Approval - Master's Thesis

Graduate College
The University of Iowa
Iowa City, Iowa

CERTIFICATE OF APPROVAL

MASTER'S THESIS

This is to certify that the Master's Thesis of

David P. Cauffman

with a major in Physics has been approved by the Examining Committee as satisfactory for the thesis requirement for the Master of Science degree at the convocation of June 7, 1968.

Thesis committee: _____
Thesis supervisor

_____
Member

_____
Member

ACKNOWLEDGEMENTS

The author is indebted to Dr. Donald Gurnett for his valuable guidance in this study, to Mr. William Taylor for many helpful discussions, and to Mrs. Dora Walker for the months she spent on various phases of the data analysis.

This research was supported in part by the Office of Naval Research under Contract No. Nonr 1509(06) and by the National Aeronautics and Space Administration under Contract No. NGR-16-001-043.

ABSTRACT

Spectrograms of very low frequency radio noise recorded by University of Iowa satellite Injun 3 at invariant latitudes greater than 50° N. are used to determine the behavior of VLF emissions during magnetic storms. The intensity of VLF emissions from L = 3 to L = 8 is studied by means of the automatic gain control levels of the satellite receiver.

It is found that for a sudden-commencement magnetic storm the VLF emission called polar chorus characteristically appears at the onset of the storm, increases in upper frequency extent to ~ 5 kHz, changes from spike to burst structure (normal chorus), occurs over the greatest area on the fourth day of the storm, subsequently fades into low frequency, spike-structure polar chorus again and eventually disappears into the ELF hiss band generally present. Chorus occurrence shows symmetry about the 9:00 - 21:00 magnetic local time meridian with a large maximum in magnetic morning and a smaller maximum in magnetic evening. Daily regions of occurrence are shown for the storm duration.

Contour maps of wide-band VLF field strength as a function of shell parameter L and universal time are presented for May through August, 1963. A correlation with D_{st} is observed.

The wide-band VLF noise intensity rises from the background noise level at the onset of a magnetic storm and peaks during the early recovery phase.

The Kennel-Petschek limiting flux hypothesis is investigated by looking for VLF noise on the appropriate L-shells when equatorial ≥ 40 keV electron fluxes reach predicted limiting values. Predicted VLF noise levels are not observed.

TABLE OF CONTENTS

LIST OF TABLES

LIST OF FIGURES

LIST OF FIGURES (CONT.)

LIST OF FIGURES (CONT.)

LIST OF FIGURES (CONT.)

Page

I. INTRODUCTION

During the past two decades studies of very low frequency (VLF) radio noise in the magnetosphere have become an active area of space research. Two principal classes of natural phenomena occur in the VLF range (1 to 30 kHz) [Cf. Gallet and Helliwell, 1959], whistlers and VLF emissions. Whistlers are VLF electromagnetic waves whose energy originates from lightning discharges and which have propagated through the magnetosphere [Storey, 1953]. VLF emissions are naturally occurring electromagnetic waves generated by energetic charged particles in the earth's magnetosphere. Only whistlers are well understood [Cf. Helliwell, 1965]. Early investigations of VLF emissions by Storey [1953] and Allcock [1957] disclosed an association between magnetic disturbances and VLF emissions. This association has been examined from ground stations by Aarons, et al. [1960], Ellis [1960], Yoshida and Hatanaka [1962a and b], Laaspere, et al. [1964], and others. Various generation mechanisms involving wave-particle interactions have been suggested for VLF emissions. See, for example, Ellis [1959], Gallet and Helliwell [1959], Ondoh [1961], Maeda and Kimura [1962], Brice [1963], and Helliwell [1967]. Generation mechanisms are discussed and classified by Brice [1964a]. Observational evidence has not yet made it possible to identify the correct mechanisms.

Ground-based studies have shown that the occurrence of VLF emissions during geomagnetic storms is principally controlled by ionospheric propagation conditions, particularly absorption and reflection at the base of the ionosphere. Satellites make possible studies of VLF phenomena which are not dominated by the propagation characteristics of the lower ionosphere. Specific advantages of a satellite study of VLF emissions include the following:

(1) Absorption is no longer a major factor in the interpretation of observations because waves are detected by the satellite before they reach the base of the ionosphere.

(2) The uncertainty in assigning an L-shell of origin to a source is reduced because the waves are detected before they enter the earth-ionosphere waveguide.

(3) Rapid surveys of the spatial extent of VLF noises are possible.

(4) A satellite has wider geographical coverage than ground stations.

(5) VLF waves trapped in the magnetosphere due to total reflection at the lower ionospheric boundary can never be observed by ground stations.

The purpose of this study is to present satellite observations of VLF emissions during magnetic storms using data from a

VLF receiver on the University of Iowa/Office of Naval Research satellite Injun 3. Two different avenues of approach are utilized. The structure of VLF emissions is studied by examining spectrograms made from frequency-time data recorded by the satellite during times of magnetic disturbance. The intensity of VLF noise is studied by means of the automatic gain control levels of the satellite receiver.

II. DESCRIPTION OF THE INJUN 3 EXPERIMENT

A brief description of the VLF experiment and relevant charged particle detectors carried by Injun 3 is presented as background for interpreting the data presented in the following sections. For a more complete discussion of the Injun 3 satellite see O'Brien, et al. [1964]. The Injun 3 VLF experiment is described more thoroughly by Gurnett and O'Brien [1964].

The University of Iowa/Office of Naval Research satellite Injun 3 was launched on 13 December 1962 into a low altitude, elliptical polar orbit having an apogee of 2785 km, a perigee of 237 km, an inclination of 70.4° to the earth's plane, and a period of 116 minutes.

Figure 1 shows a block diagram of the Injun 3 VLF experiment. The magnetic component of the VLF electromagnetic wave is detected by a 12" diameter loop antenna composed of 50 turns of #16 copper wire and oriented with its axis perpendicular to the direction of the geomagnetic field line. Figure 2 shows the loop antenna. An automatic gain control (AGC) circuit in the receiver compresses the signal from the loop antenna to a constant amplitude. The signals are then telemetered to tracking stations on the ground, where they are tape-recorded for later analysis with

spectrum analyzing equipment such as the Rayspan spectrum analyzer. The AGC feedback voltage is telemetered to the ground also, as a measure of wide-band VLF magnetic field intensity. The noise threshold for the wide-band field strength measurement is $\sim 10^{-13}\gamma$ ($1\ \gamma = 10^{-5}$ gauss). The satellite wide-band receiver has a frequency range of approximately 0.2 to 7.0 kHz. Figure 3 illustrates the frequency response of the Injun 3 receiver.

Data from two charged particle detectors are used in this study. Detectors 1 and 5 are both 213-type geiger tubes with an energy threshold of $\sim$ 40 keV for electrons, and $\sim$ 500 keV for protons. Detector 1 is oriented to detect particles moving perpendicular to the local geomagnetic field line (pitch angle $\alpha \simeq 90°$). The geometric factor of detector 1 is 0.6×10^{-2} cm^2 ster [Craven, 1966; Frank et al., 1964]. Detector 5 is oriented to detect particles moving parallel to the local magnetic field line (pitch angle $\alpha \simeq 0°$), downwards in the northern hemisphere. The geometric factor of detector 5 is 5.0×10^{-2} cm^2 ster [Fritz, 1968].

Computations and machine plots used in this study were done on an IBM 7044 computer and a Univac 418 computer with a Calcomp plotter.

III. STRUCTURE OF VLF EMISSIONS DURING MAGNETIC STORMS

Gallet [1959] divided VLF noises into three broad classes: whistlers, emissions, and interactions between whistlers and emissions. Helliwell [1965] gives a classification scheme for VLF emissions involving the following principal categories: hiss, chorus, discrete emissions, triggered emissions, periodic emissions, and quasi-periodic emissions. In this study three types of emissions are examined: VLF hiss, ELF hiss, and chorus. Incoherent, band limited white noise with a duration of minutes and with little temporal structure on a time scale less than one second is called hiss. If there are frequency components from a few hundred Hz to about 2 kHz it is called extremely low frequency (ELF) hiss; otherwise it is called VLF hiss. ELF hiss generally occurs in bands about 1 kHz wide during local daytime at middle and high latitudes. Chorus is a sequence of discrete emissions occurring randomly in time and generally rising in frequency on a time scale of a few tenths of a second. Ungstrup and Jackerott [1963] distinguish between normal chorus, previously called dawn chorus [Storey, 1953], which occurs mostly at middle latitudes and at frequencies above 2 kHz, and polar chorus, which occurs mostly at high latitudes and below 2 kHz. Polar chorus commonly occurs with one or more ELF hiss bands. The periodic emissions we observe which are not clearly

whistler-related generally resemble chorus, and are classified as chorus. The spectrogram in Figure 4 shows examples of VLF hiss (minutes 23-24), polar chorus with an ELF hiss band (minutes 29-31), and normal chorus (minutes 14-17). Figure 5 shows another variation of normal chorus (minutes 52-53) as well as polar chorus unaccompanied by ELF hiss (minute 50).

The three coordinates used in analyzing the data are universal time (UT), invariant latitude (INV), and magnetic local time (MLT). Following Gurnett and O'Brien [1964] we have made the assumption that altitude is not an important parameter. Invariant latitude is defined by the relation:

$$\text{INV} = \arccos \frac{1}{\sqrt{L}}$$

where L is the shell parameter of McIllwain [1961]. Magnetic local time is defined as the hour angle between the magnetic meridian through the satellite and the magnetic meridian through the sun, using the centered dipole approximation [Chamberlain, 1961]. The data available are classified by MLT-INV "sector". Sector 3-60, for example, includes data between 3 and 4 hours MLT and between 60° and 70° INV. The same sector size, 1 hour MLT by 10° INV, is used throughout the paper.

Five sudden-commencement magnetic storms, one magnetic enhancement, and one "quiet time" were chosen for study from the Injun 3 data on the basis of the quantity and quality of data available. Table 1 lists these periods, gives the sudden commencement times of storms [Lincoln, 1964a and b], and indicates the number of MLT-INV sectors of each period for which data were assembled and analyzed.

The method of data analysis is straightforward. Satellite orbit plots such as those in Figures 6 and 7 were used to select sectors for which data were available during each day of the storm. Using a Rayspan spectrum analyzer, frequency-time spectrograms were produced for all passes through these sectors. A visual analysis was made of the types of VLF emissions observed each day in the spectrograms of each sector.

Several explanatory remarks about the data reduction are in order:

(1) Only phenomena which were clearly present were counted in performing the visual analysis of the spectrograms; dubious phenomena were ignored. Rates of occurrence found for phenomena are therefore always minimum rates.

(2) A fuzzy fringe commonly occurs on the top edge of ELF hiss bands. This fringe is counted as chorus only if the components

are clearly distinguishable on the 0.5 mm/sec low time resolution spectrograms. An example of such a fringe which would not be called chorus is discernable in Figure 4 (minutes 32-36).

(3) Spectrograms give no information about the absolute intensity of VLF radio noise. Due to the AGC feature of the satellite receiver, spectrograms are produced with maximum contrast between phenomena occurring over a range of frequencies at a particular instant, but the gain variations involved preclude evaluating the relative intensities of phenomena at different times.

(4) Of approximately twelve satellite revolutions per day, an average of two spectrograms per sector per day contain usable data, due partly to the difference in satellite trajectory from one revolution to the next in MLT-INV coordinates and partly to the variable quality of data from some of the receiving stations.

(5) Variation in the number of passes per sector per day could influence the probability that a phenomenon be observed and affect the occurrence results. However, variation in the length of time spent by the satellite in each sector will not usually influence the results because the duration of the emission phenomena at one location is generally greater than a few minutes, although often less than two hours. It will be shown later that variation

in the number of passes per sector per day does not significantly distort the gross features of the results.

Figures 8 through 12 illustrate selected parts of the data from five storm sectors which exhibit representative behavior. Visual examination of such sector charts reveals the following:

(1) ELF hiss is present in most sectors most of the time, including pre-storm times.

(2) VLF hiss is present occasionally with no apparent temporal pattern.

(3) Chorus appears after the storm sudden commencement. Its upper limit may increase to frequencies of ~ 5 kHz, its nature may change from a spike to a burst structure, and it frequently becomes a periodic emission [Cf. Helliwell, 1965] having recurrent spectral forms on intervals of the order of 10 seconds. High-frequency, burst-type, possibly periodic chorus is observed from the second through the fourth days of a storm, after which the chorus returns to lower frequencies, reverts to spike structure, and eventually fades into the ELF hiss background normally present. Figure 4 shows examples of both burst-type chorus (minutes 15-17) and spike-type chorus (minute 40).

Tables 2 through 8 list the results of the sector analysis, indicating whether VLF hiss, ELF hiss, or chorus was observed to

occur in each sector during each day of each period. During the quiet period ELF hiss was a common occurrence and a few cases of polar chorus were observed. During the July 30 magnetic enhancement ELF hiss was observed almost continually, some VLF hiss occurred, and a few occurrences of polar chorus were observed. These results confirm that the chorus frequently observed during magnetic storms is associated with the occurrence of the magnetic storms.

Figure 13 shows the time development of chorus, averaged over sectors, for the 30 April, 6 June, and 18 August magnetic storms, for which the most data were available. In two of these storms (30 April and 6 June) the behavior of chorus is very similar, occurring in over 80% of the sectors on the fourth day of the storms. Chorus never occurs in more than 40% of the sectors during the 18 August storm, probably because the data comes from evening MLT sectors only, where VLF emissions are least often observed.

In the analysis which follows, data for corresponding sectors and days of the different storms is summed. Since each storm contributes sectors on a different section of the polar magnetic map due to precession of the satellite orbit about the magnetic pole, this procedure allows us to construct a general picture of what "characteristically" happens in the vicinity of the magnetic pole during magnetic storms.

Figure 14 shows the time development of chorus, VLF hiss, and ELF hiss averaged for the five storms. The rate of occurrence of ELF hiss is high throughout the storms, and constant to within our confidence limits. The "average confidence" of the results is taken simply as $\sqrt{N}/N$ where N is the average number of sectors for which data was added in order to assign an occurrence rate to one day. The confidence is similar for all points in the figure. The rate of occurrence of VLF hiss is low, and while it appears to increase with the onset of the storm, the statistics of this study do not permit us to say so with certainty. The frequency of occurrence of chorus, however, shows a significant increase after the onset of the storm, with a maximum on the fourth day of the storm.

Figure 15 shows the occurrence of chorus in MLT-INV coordinates summed over all days of five storms. Symmetry about the 9:00 - 21:00 MLT meridian is apparent, as is a "compression" of the pattern on the morning side, pushing it to higher invariant latitudes than on the evening side. An unexpected set of "nulls" at 1 and 17 hours MLT is observed, defining an evening peak centered on 21 hours MLT. In Figure 16 the patterns of occurrence of chorus (summed over five storms) are shown for each day from two days before, to the sixth day after, the storm sudden commencement. The observations made from Figures 13 and 15 are apparent in Figure 16.

Approximate symmetry about the 9:00 - 21:00 MLT meridian is maintained and the greatest geographical coverage of chorus occurs on the fourth day. The main (morning) lobe of chorus does not appear until the second day of the storm and has broken up on the sixth day. A temporary breakup occurs on the third day. The evening lobe, which we first observe on the second day, remains through at least the sixth day of the storm. Its disappearance on the fifth day is probably due to lack of data in the evening region.

Two individual passes were chosen for detailed examination because of the variety and contrast of data they display. Figures 4 and 5 show spectrograms of these passes, together with VLF wide-band magnetic field intensity, trapped and precipitated $\geq$ 40 keV electron fluxes, and satellite orbit parameters. Orbits for the two passes in magnetic polar coordinates are shown in Figures 6 and 7. In Figure 4 a distinction in region of occurrence between VLF hiss and chorus is evident. VLF hiss is observed above the $\geq$ 40 keV electron trapping boundary. Chorus, however, is observed at invariant latitudes below the trapping boundary at both magnetic morning and noon ends of the pass. ELF hiss is observed throughout the pass. A comparison of the spectrograms with the AGC level indicates that ELF hiss is the strongest phenomenon

observed, reaching a maximum intensity at about 11 hours MLT and 70° INV (minute 35). The precipitated ≥ 40 keV electron flux peaked at the same time. Figure 5 shows that burst-type, normal chorus can occur in magnetic evening during a storm as well as in magnetic morning. The sudden cut-off of chorus activity at 14 hours 53 minutes 26 seconds corresponds to a reduction in the precipitated ≥ 40 keV electron flux. This cut-off is probably due to the phenomenon of the plasmapause [Carpenter, 1966]. No VLF hiss or ELF hiss is observed during this pass.

A definitive statement about the differences between the types of chorus generally observed in magnetic morning and in magnetic evening is not possible because none of the storms considered involved data from both local time regions.

We shall now discuss further the results just presented and compare them with the findings of other investigators. The observation of normal chorus during the first four days of magnetic storms is consistent with the results of Storey [1953] and Allcock [1957], who find that middle latitude (normal) chorus correlates positively with magnetic activity. Crouchley and Brice [1960] and Ungstrup and Jackerott [1963] report a negative correlation of polar chorus, as seen from the ground, with magnetic activity. We infer a positive correlation. This apparent discrepancy is removed by the

hypothesis of Pope [1959, 1963] that the negative correlation is due to ionospheric absorption, which is not an important factor in the satellite observations. Helliwell [1965] offers evidence in support of this interpretation. Ungstrup and Jackerott [1963] report also that polar chorus often disappears during disturbed periods. Our observations confirm this.

It has been found that chorus occurrence peaks in MLT at dawn at middle latitudes and that the peak spirals towards noon at high latitudes [Ondoh, 1961; Pope, 1963]. The broad peak we observe centered on 9 hours MLT at high latitudes does not seriously disagree with this, and a slight discrepancy may be expected due to the effect reported by Laaspere, et al. [1964], who find that disturbed day chorus peaks earlier than quiet day chorus. The 9 hours MLT result for the position of the diurnal maximum is consistent with the results of a 1963 ground station study by Jørgensen [1965] and with a statistical study using Injun 3 data by Oliven and Gurnett [1968]. Brice [1964b] offers a theoretical explanation for this diurnal variation. An evening peak in chorus occurrence was discovered in Australia by Crouchley and Brice [1960] using ground station data.

If we compare the pattern of chorus occurrence indicated by the dashed line in Figure 15 with the boundary for trapped

≥ 40 keV electron fluxes of Frank et al. [1964], we note that the high latitude cut-off for chorus has approximately the same shape as the particle trapping boundary and that chorus occurs on the low latitude side of the trapping boundary. VLF hiss has been shown by Gurnett [1966] to occur on the high latitude side of the trapping boundary. These generalizations are consistent with the individual pass data shown in Figure 4.

It has been mentioned that variation in the average number of passes through a sector which were analyzed for each day of the storm may affect the probability of detecting a phenomenon and hence distort the occurrence results. Figure 17 shows the number of passes per sector (averaged over all the sectors for which data were analyzed) versus day of storm. Comparison with the data in Figure 13 and 14 reveals no systematic correlation; while some maxima in the number of passes per sector coincide with peaks in the data, others coincide with minima in the data. We conclude that the variation in the number of passes per sector does not significantly distort the gross features of our results.

IV. INTENSITY OF VLF EMISSIONS

The VLF radio noise intensity in the frequency range 0.2 to 7.0 kHz is studied by means of the AGC feedback voltage. The objective of this portion of the study is to produce contour maps of constant wide-band VLF field strength (AGC) on L versus UT axes. A description of the procedure follows. AGC readings are available every four seconds during a satellite pass over a receiving station. Only northern hemisphere data with $3 \leq L \leq 8$ and 28 April $\leq$ UT $\leq$ 28 August (1963) were used, since the density of data was too low outside these limits. That 4 second AGC reading which was nearest to, but at higher latitude than, each 0.2 L increment was selected for each revolution (REV). The resulting grid of AGC values, one for each 0.2 L by 1 REV block, is called a preliminary AGC map. The highest AGC value for each 0.2 L increment during each day was selected as the grid point for that 0.2 L by 1 day block. Contours of constant AGC were drawn on the grid thus created. These final maps are reproduced in Figures 18 and 19.

The analysis was performed separately for northbound and southbound passes because these occurred at substantially different magnetic local times, as can be seen from Figure 6, which shows

a typical orbit in magnetic coordinates. Even on a northbound or a southbound map, data for any one day may come from within about a 6-hour MLT range.

The preliminary maps were initially reduced to a different set of final maps by averaging the corresponding points for all revolutions during one day. Because the intensity of VLF noise fluctuates on a time scale usually less than two hours (one revolution) the averaging process removes many features of the maps. To retain these features and to facilitate the comparison described in Section V of this paper, selection of the maximum AGC is preferable.

Another set of preliminary maps has been made on INV versus UT axes at 2° intervals for $50° \leq INV \leq 82°$. Data density for these maps is more uniform than for those on L versus UT coordinates because the speed at which the satellite "scans" the maps is nearly constant. However, differences between the two sets of maps do not seem important in the range $3 \leq L \leq 8$, which includes most of the features of the data, and L is a more useful coordinate than INV for comparisons with particle fluxes.

The preliminary maps themselves were not satisfactory because data were rarely available for more than a few of the 12 possible revolutions per day. However, these relatively fast time

scale data were useful in clarifying details of boundaries on the final maps.

The largest error in the production of the maps is the error introduced in drawing the contours. A reasonable standard deviation for the positions of the lines drawn is 0.2 L by 1 day. That is, we believe another experimenter analyzing the same data by the same guidelines would agree with us to within one grid point. The guidelines adopted were the following:

(1) Single points are ignored unless they fit into a larger trend of the data.

(2) Details of contours (for instance, whether two close peaks should be joined) may depend on a single point only if such dependence is clearly substantiated by the preliminary (fast time scale) maps.

The result of the application of these guidelines is to remove from the maps variations on a time scale of one day or less, or on an L scale of 0.2 or less. The extent of "active" areas will in general exceed that indicated, since lines through regions of sparce data have been drawn conservatively.

The utility of this method of presenting the data may be emphasized by pointing out that the contours presented in Figures 18 and 19 summarize about 10^5 4-second experimental measurements.

Given below is a summary of observations of wide-band field strength made from the INV versus REV, L versus REV, and L versus UT contour maps. The last set is reproduced in Figures 18 and 19.

(1) Contour peaks center on about 63° INV ($L \simeq 5$).

(2) Most regions of activity extend northward to about 75° INV, and few regions exceed this limit. We call this 75° INV limit an average maximum northern extent of activity.

(3) Activity extends below 50° INV, which was the lowest latitude for which data were analyzed.

(4) Rough MLT dependence can be investigated by comparison of data taken during northbound passes with data taken during southbound passes. Regions of high AGC appear largest during forenoon MLT (6 to 12 hours) and smallest during evening MLT (18 to 24 hours).

(5) Continuity was observed in latitude readings; that is, peaks fade gradually on both sides.

(6) Little continuity is observed in the data between revolutions. The time scale of the details of the phenomena is less than two hours.

(7) Correspondence with magnetic index K_p is fair. Each peak with $K_p \geq 4$ can be associated with a major peak or region of enhancement on the AGC maps, although the converse is not true. Also,

periods indicated to be quiet by K_p are generally quiet in radio noise intensity. In comparing the AGC maps with K_p and D_{st} it must be kept in mind that the maps will reflect local substorms which may not be reflected in the planetary averages K_p and D_{st}.

(8) Correspondence with the horizontal component D_{st} is good. Major fluctuations in D_{st} can nearly always be associated with increases in wide-band field strength, and, unlike the correspondence with K_p, the details of small fluctuations in D_{st} often appear to be reflected in the AGC readings.

(9) Three sudden commencement magnetic storms occurred during the period for which AGC maps have been made. These occurred on 30 April, 6 June, and 18 August (Cf. Table 1). The wide-band VLF field strength rises above background noise at the onset of the storm, grows during the initial and main phases, and peaks during the early recovery phase. The first two storms are of the standard type [Cf. Akasofu, 1966] and show this effect clearly, but the 18 August storm has no clearly defined main phase.

The results just presented will now be discussed further and compared with the findings of other investigators. Figure 20 reproduces the frequency of occurrence distribution of VLF emissions observed by Injun 3 found in a statistical study by Taylor and Gurnett [1968]. There is good agreement with the observation made from the AGC maps of a magnetic morning maximum at about 63° INV.

An average maximum northern extent of activity at 75° INV is also consistent with Taylor and Gurnett's results.

ELF hiss is the strongest and most common emission observed by Injun 3 [Taylor and Gurnett, 1968], and little error is made if the maps of wide-band field strength are assumed to reflect the intensity of ELF hiss. Comparison of the wide-band field strength contour maps with the equatorial omnidirectional ≥ 40 keV electron flux contours of Owens and Frank [1968] (Cf. Figure 21) discloses no more agreement than would be expected due to the general correlation of the two phenomena with K_p.

Tokuda [1962] and others have previously reported that VLF emission activity correlates with the horizontal component of the geomagnetic field.

V. INVESTIGATION OF THE KENNEL-PETSCHEK HYPOTHESIS

Kennel and Petschek [1966a and b] have proposed a model for wave-particle interactions which predicts a limiting flux for given energy trapped particles due to energy losses to whistler mode noise. The limiting equatorial flux J^* for ≥ 40 keV electrons is predicted to be

$$J^* \approx \frac{7 \times 10^{10}}{L^4} \quad (\text{cm}^2 \text{ sec})^{-1} .$$

The Kennel-Petschek model predicts that when the equatorial electron flux J is greater than J^* on a given L shell, VLF noise will be generated. This noise will in general propagate along the magnetic lines of force of that L shell to the earth. The equatorial strength of the noise should be of the order of $10^{-2}\gamma$. Away from the equator some attenuation can be expected due to non-ideal propagation conditions.

Values of equatorial ≥ 40 keV omnidirectional electron fluxes obtained with the Explorer 14 satellite are given by Owens and Frank [1968]. Omnidirectional electron flux is approximately equal to trapped electron flux. Electron fluxes

and VLF noise intensity data are both available for May, June, and July of 1963. During the latter two months electron fluxes exceeded the limiting flux by small margins five times. Figure 21 shows electron intensity contours, regions of $J \geq J^*$, and wide-band field strength contours.

The correspondence of $J \geq J^*$ regions to AGC peaks is not good. Selecting VLF data taken in the morning quadrant of MLT, we can identify a radio noise intensification region with each $J \geq J^*$ region. However, centers of the VLF noise regions are about two L-shells lower than centers of the $J \geq J^*$ regions, and the outlines have little in common. Only one of the correspondent VLF regions has a magnitude as high as $8 \times 10^{-3}\gamma$.

While the data do not provide much support for the Kennel-Petschek hypothesis, they cannot be regarded as conclusive evidence against it. The major unknown remaining in the problem is the set of propagation conditions between the generation region at the equator and the satellite position near the poles. The following possibilities remain:

(1) Assume that the wave attenuation factor is $\leq 10^{-1}$. The expected wave intensity is then reduced to below the Injun 3 receiver background noise level.

(2) Assume that the wave attenuation factor is $\sim \frac{1}{2}$ and also assume some mechanism for shifting the waves to lower L values.

Our data and such a mechanism would constitute a strong support for the model.

(3) Assume that the noise generated was limited to frequencies greater than 7 kHz, the upper limit of the Injun 3 receiver, or less than 1 kHz. The wide-band field strength measurement was calibrated using a white noise source which caused all frequency components to be weighted equally. Because the receiver frequency response is not flat (see Figure 3), the AGC reading will give an incorrect field strength measurement if the magnetic field noise spectrum is not flat. As the frequency of the peak spectral contribution decreases below 1 kHz, the error (a low AGC reading) rapidly increases from ~ 4 db.

(4) Reject the Kennel-Petschek hypothesis.

Some combination of the first and third possibilities is probably the most reasonable solution. Thorne and Kennel [1967] have pointed out that waves which reach low altitudes will have predominantly electric rather than magnetic fields and can account for the low VLF noise levels observed with Injun 3. However, the OGO-I VLF/LF experiment by Stanford [Dunckel and Helliwell, 1966] reports magnetic intensities in the equatorial plane very similar to those reported by us at high latitudes. It is unlikely that Injun 3 simply missed the noise; three of the $J \geq J^*$ regions

occurred with the satellite traversing the morning MLT quadrant, where VLF noise is most likely to be observed.

A more significant test of the hypothesis could be made with simultaneous particle and VLF measurements in the vicinity of L = 6 at the magnetic equator.

TABLE 1

Periods Studied

Period Type	Date (1963)	Sudden Commencement (MO-HR MIN)	Data Analyzed		Number of Sectors Analyzed
			Dates	Satellite Revolution Nos.	
Magnetic Storms	April 4	04-0546	April 3 - 9	1379-1462	3
	April 30	30-1522	April 29 - May 7	1700-1812	8
	June 6	06-1511	June 5 - 11	2164-2247	18
	August 18	18-0816	August 15 - 24	3051-3175	13
	September 13	13-1925	September 12 - 30	3402-3514	2
Magnetic Enhancement	July 30		July 28 - August 3	2826-2912	13
Quiet Time	August 11		August 11 - 13	3001-3038	12

TABLE 2

April 4 Magnetic Storm Sector Analysis

MLT-INV Sector	April 4	5	6	7	8	9
1 - 50						
23 - 50		C				
22 - 60	H	EC	H		H	

H VLF hiss (> 2 kHz)

E ELF hiss (< 2 kHz)

C chorus

X no data

TABLE 3

April 30 Magnetic Storm Sector Analysis

MLT - INV Sector	April 29	30	May 1	2	3	4	5	6	7
18 - 50	E	X	E	E	C	X	EC	EC	EC
9 - 60	H	X	EC	EC	EC	EC	EC	E	EC
17 - 60	X	X	E	X	EC	E	E	X	EC
18 - 60	E	X	X	E	X	E	EC	X	X
11 - 70		X	E	E	HEC	E	E	E	E
14 - 70	E	X	X	HE	HEC	H	HE	E	E
15 - 70	E	X	H	HE	EC	H	E	E	E
16 - 70	E	X		E	E	H	EC	E	E

H VLF hiss (> 2 kHz)

E ELF hiss (< 2 kHz)

C chorus

X no data

TABLE 4

June 6 Magnetic Storm Sector Analysis

MLT - INV Sector	June 4	5	6	7	8	9	10	11
3 - 50	H		EC	EC		C		
4 - 50	X			E	EC	C	EC	
2 - 60	H	H	HE	X	EC	EC		
3 - 60	H	H	EC	X	X	EC		EC
4 - 60	X	E		EC		EC	EC	EC
5 - 60				EC	EC	C	EC	EC
6 - 60				EC	EC	EC	EC	EC
7 - 60					E	EC	EC	E
8 - 60		E		X	E	X	E	E
9 - 60			X	X	E	EC	EC	X
10 - 60		E	X	EC	X	EC	EC	EC
11 - 60		X	E	EC	X	EC	EC	EC
5 - 70	EC		E	HE	X	EC		E
6 - 70			E	HE	X	EC		EC
7 - 70	E	E	E	EC	X	EC	E	E
8 - 70	E	E	E	HEC	X	EC	EC	E
9 - 70	E	E	E	EC	X	EC	HEC	E
10 - 70	EC	X	E	E	X	EC	HEC	EC

TABLE 5

August 18 Magnetic Storm Sector Analysis

MLT - INV Sector	August 15	16	17	18	19	20	21	22	23	24
13 - 50	E	E	E	HEC	EC	EC	EC	X	HE	X
13 - 60	X	X	E	EC	EC	EC	EC	EC	EC	E
14 - 60	E	E	EC	EC	EC	E	E	X	HE	X
21 - 60	X	HE	E	E	X	HC	C	X	HEC	E
22 - 60	E	HE	E	EC	E	HEC	HC	HE	E	H
14 - 70	E	E	E	E	EC	E	E	E	E	X
15 - 70	E	HE	E	X	E	E	HE	E	X	X
16 - 70	E	HE	E	E	E	X		X		E
17 - 70	E	X	HE	HE		E		X		E
18 - 70	E	X	X	HE	E	E	H	X	E	E
19 - 70	E	E	X	E	E	E	H	E	E	E
20 - 70	E	E	X	E	E	HE	H	E	E	HE
21 - 70	E	E	X	E	X	E	HE	EC		H

TABLE 6

September 13 Magnetic Storm Sector Analysis

MLT - INV Sector	Sept. 12	13	14	15	16	17	18	19	20
17 - 50		C		X		E	X	E	E
16 - 60	E	X		X	E	E	X	E	

H VLF hiss (> 2 kHz)

E ELF hiss (< 2 kHz)

C chorus

X no data

TABLE 7

July 30 Magnetic Enhancement Sector Analysis

MLT - INV Sector	July 28	29	30	31	August 1	2	3
16 - 50	X		E	E	E	E	EC
2 - 60	X		E	EC	EC	HE	C
17 - 60	E	E	E	HE	E	E	E
0 - 70	E	E	E	E	E	E	E
1 - 70	E		E	HE	E	E	
17 - 70	E		HE	E	E	HE	E
18 - 70	E		E	E		E	E
19 - 70	HE		E	E	E	X	E
20 - 70	X		E	E	E	X	E
21 - 70	HE	E	E	E	E	X	HE
22 - 70	HE	E	E	HE	E	X	HE
23 - 70	X	E	E	HE	E	E	HE
(0-6)- 80	E	X	E	E		E	

H VLF hiss (> 2 kHz)

E ELF hiss (< 2 kHz)

C chorus

X no data

TABLE 8

August 11 Quiet Period Sector Analysis

MLT - INV Sector	August 11	12	13
14 - 50	E	E	E
15 - 50	E	E	E
14 - 60	EC	EC	E
15 - 60	EC	E	EC
16 - 60	X	E	E
17 - 60	X	EC	E
15 - 70	EC	E	HE
16 - 70	E	E	E
17 - 70			
18 - 70		E	
19 - 70		E	
20 - 70		E	

H VLF hiss (> 2 kHz)

E ELF hiss (< 2 kHz)

C chorus

X no data

REFERENCES

Aarons, J., G. Gustafsson, and A. Egeland, "Correlation of audio-frequency electromagnetic radiation with auroral zone micropulsations," Nature 185, 148-151 (1960).

Akasofu, S., "Electrodynamics of the magnetosphere: Geomagnetic storms," Dept. of Physics and Astronomy, Univ. of Iowa, Iowa City, Iowa, Res. Rept. 66-19 (1966).

Allcock, G. McK., "A study of the audio-frequency radio phenomenon known as 'dawn chorus'," Australian J. Phys. 10 (2), 286-298 (1957).

Brice, N., "An explanation of triggered very low frequency emissions," J. Geophys. Res. 68 (15), 4626-4628 (1963).

Brice, N., "Fundamentals of very low frequency emission generation mechanisms," J. Geophys. Res. 69 (21), 4515-4522 (1964).

Brice, N., "A qualitative explanation of the diurnal variation of chorus," J. Geophys. Res. 69 (21), 4701-4703 (1964).

Carpenter, D. L., "Whistler studies of the plasmapause in the magnetosphere, 1, Temporal variations in the position of the knee and some evidence on plasma motions near the knee," J. Geophys. Res. 71 (3), 693-710 (1966).

Chamberlain, J. W., Physics of the Aurora and Airglow (Academic Press, New York, 1961).

Craven, J. D., "Temporal variations of electron intensities at low altitudes in the outer radiation zone as observed with satellite Injun 3," J. Geophys. Res. 71 (23), 5643-5663 (1966).

Crouchley, J. and N. M. Brice, "A study of 'chorus' observed at Australian stations," Planet. Space Sci. 2 (4), 238-245 (1960).

Dunckel, N. and R. A. Helliwell, "Whistler and VLF emission intensities observed in the magnetosphere by the OGO-I satellite," paper no. 4-4-3 presented at the U.R.S.I. spring meeting, Washington, D. C. (1966).

Ellis, G. R. A., "Low frequency electromagnetic radiation associated with magnetic disturbances," Planet. Space Sci. 1, 253-258 (1959).

Ellis, G. R. A., "Geomagnetic disturbances and 5 kcps electromagnetic radiation," J. Geophys. Res. 65 (6), 1705-1710 (1960).

Frank, L. A., J. A. Van Allen, and J. D. Craven, "Large diurnal variations of geomagnetically trapped and of precipitated electrons observed at low altitudes," J. Geophys. Res. 69 (15), 3155-3167 (1964).

Fritz, T. A., "Spectral, spatial, and temporal variations observed for outer zone electrons from 10 to 100 keV with satellite Injun 3," J. Geophys. Res. (to be published) (1968).

Gallet, R. M., "The very low frequency emissions generated in the earth's exosphere," Proc. IRE 47 (2), 211-231 (1959).

Gallet, R. M., and R. A. Helliwell, "Origin of very low frequency emissions," J. Res. Natl. Bur. Std. 63D (1), 21-27 (1959).

Gurnett, D. A., "A satellite study of VLF hiss," J. Geophys. Res. 71 (23), 5591-5615 (1966).

Gurnett, D. A. and B. J. O'Brien, "High latitude studies with satellite Injun 3; Part 5, Very low frequency electromagnetic radiation," J. Geophys. Res. 69 (1), 65-89 (1964).

Helliwell, R. A., Whistlers and Related Ionospheric Phenomena, (Stanford Univ. Press, Stanford, California, 1965).

Helliwell, R. A., "A theory of discrete VLF emissions from the magnetosphere," J. Geophys. Res. 72 (19), 4773-4790 (1967).

Jørgensen, T. S., Technical (final) report, "Observations of whistlers and VLF emissions at Godhaven and Narssarssauq, Greenland and Tromsø, Norway in 1963," Ionosphere Laboratory, The Technical Univ. of Denmark, Lyngby, Denmark (1965).

Kennel, C. F. and H. E. Petschek, "Limit on stably trapped particle fluxes," J. Geophys. Res. 71 (1), 1-28 (1966).

Kennel, C. F. and H. E. Petschek, "Van Allen belt plasma physics," Avco-Everett Res. Rept. 259 (1966).

Laaspere, T., M. G. Morgan, and W. C. Johnson, "Chorus, hiss, and other audio-frequency emissions at stations of the Whistlers-East network," Proc. IEEE 52, 1331-1349 (1964).

Lincoln, J. V., "Geomagnetic and solar data," J. Geophys. Res. 69 (3), 525-529 (1964).

Lincoln, J. V., "Geomagnetic and solar data," J. Geophys. Res. 69 (9), 1903-1909 (1964).

Maeda, K. and I. Kimura, "Origin and mechanism of VLF emissions," Space Sci. Res. 3, (W. Priestler, ed.; John Wiley and Sons, New York, 1962).

McIllwain, C. E., "Coordinates for mapping the distribution of magnetically trapped particles," J. Geophys. Res. 66, 3681-3691 (1961).

O'Brien, B. J., C. D. Laughlin, and D. A. Gurnett, "High latitude geophysical studies with satellite Injun 3; Part 1, Description of the satellite," J. Geophys. Res. 69 (1), 1-12 (1964).

Oliven, M. N. and D. A. Gurnett, "Microburst phenomena 3. An association between microbursts and VLF chorus," J. Geophys. Res. 73 (7), 2355-2362 (1968).

Ondoh, T., "On the origin of VLF noise in the earth's exosphere," J. Geomag. and Geoelec. 12 (2), 77-83 (1961).

Owens, H. D. and L. A. Frank, "Electron omnidirectional intensity contours in the earth's outer radiation zone at the magnetic equator," J. Geophys. Res. 73 (1), 199-208 (1968).

Pope, J. H., "An investigation of whistlers and chorus at high latitudes," Sci. Rept. No. 4, Air Force Contract No. AF19(604)-1859, 1-38, Geophys. Inst. Univ. of Alaska, College, Alaska (1959).

Pope, J. H., "A high-latitude investigation of the natural very low frequency electromagnetic radiation known as chorus," J. Geophys. Res. 68(1), 83-99 (1963).

Storey, L. R. O., "An investigation of whistling atmospherics," Phil. Trans. Roy. Soc. London 246 (908), 113-141 (1953).

Taylor, W. W. L. and D. A. Gurnett, "The morphology of VLF emissions observed with the Injun 3 satellite," J. Geophys. Res. (to be published) (1968).

Thorne, R. M. and C. F. Kennel, "Quasi-trapped VLF propagation in the outer magnetosphere," J. Geophys. Res. 72 (3), 857-870 (1967).

Tokuda, H., "VLF emissions and geomagnetic disturbances at the auroral zone; Part 1, Chorus bursts and preceding geomagnetic disturbances," J. Geomag. and Geoelec. 14 (1), 33-40 (1962).

Ungstrup, E. and I. M. Jackerott, "Observations of chorus below 1500 cycles per second at Godhaven,Greenland, from July 1957 to December, 1961," J. Geophys. Res. 68 (8), 2141-2146 (1963).

Yoshida, S. and T. Hatanaka, "The disturbances of exosphere as seen from the VLF emission," J. Phys. Soc. Japan 17 (suppl. A-II), 78-83 (1962).

Yoshida, S. and T. Hatanaka, "Variations in the VLF emissions with reference to the exosphere," Rept. Iono. Space Res. Japan 16 (4), 387-409 (1962).

FIGURE 1. Block diagram of the Injun 3 VLF experiment.

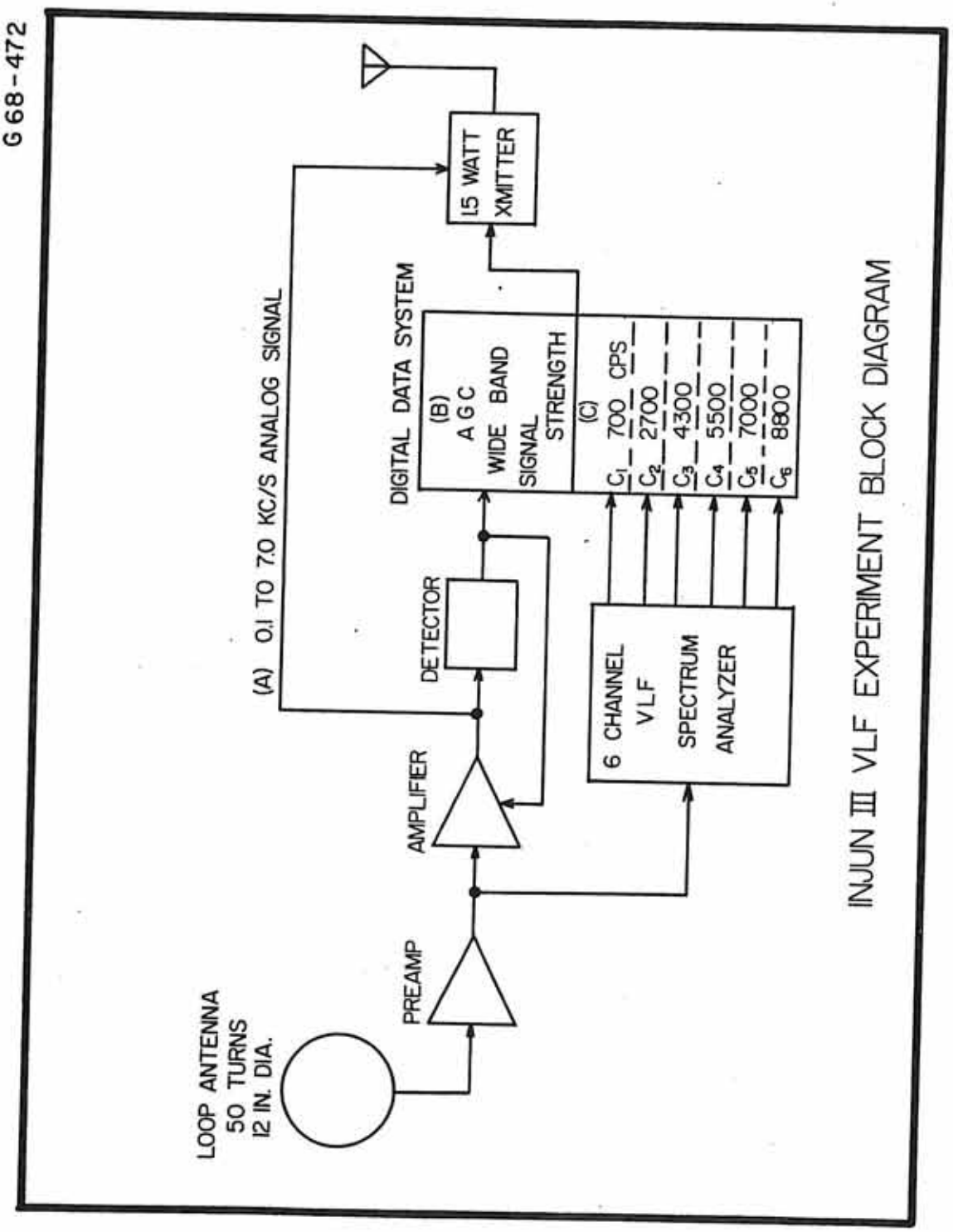
G 68-472
INJUN III VLF EXPERIMENT BLOCK DIAGRAM
LOOP ANTENNA
50 TURNS
12 IN. DIA.
PREAMP
AMPLIFIER
DETECTOR
(A) 0.1 TO 7.0 KC/S ANALOG SIGNAL
6 CHANNEL
VLF
SPECTRUM
ANALYZER
DIGITAL DATA SYSTEM
(B)
A G C
WIDE BAND
SIGNAL
STRENGTH
(C)
C1 700 CPS
C2 2700
C3 4300
C4 5500
C5 7000
C6 8800
15 WATT
XMITTER

FIGURE 1

FIGURE 2. Photograph of the Injun 3 satellite showing the VLF loop antenna.

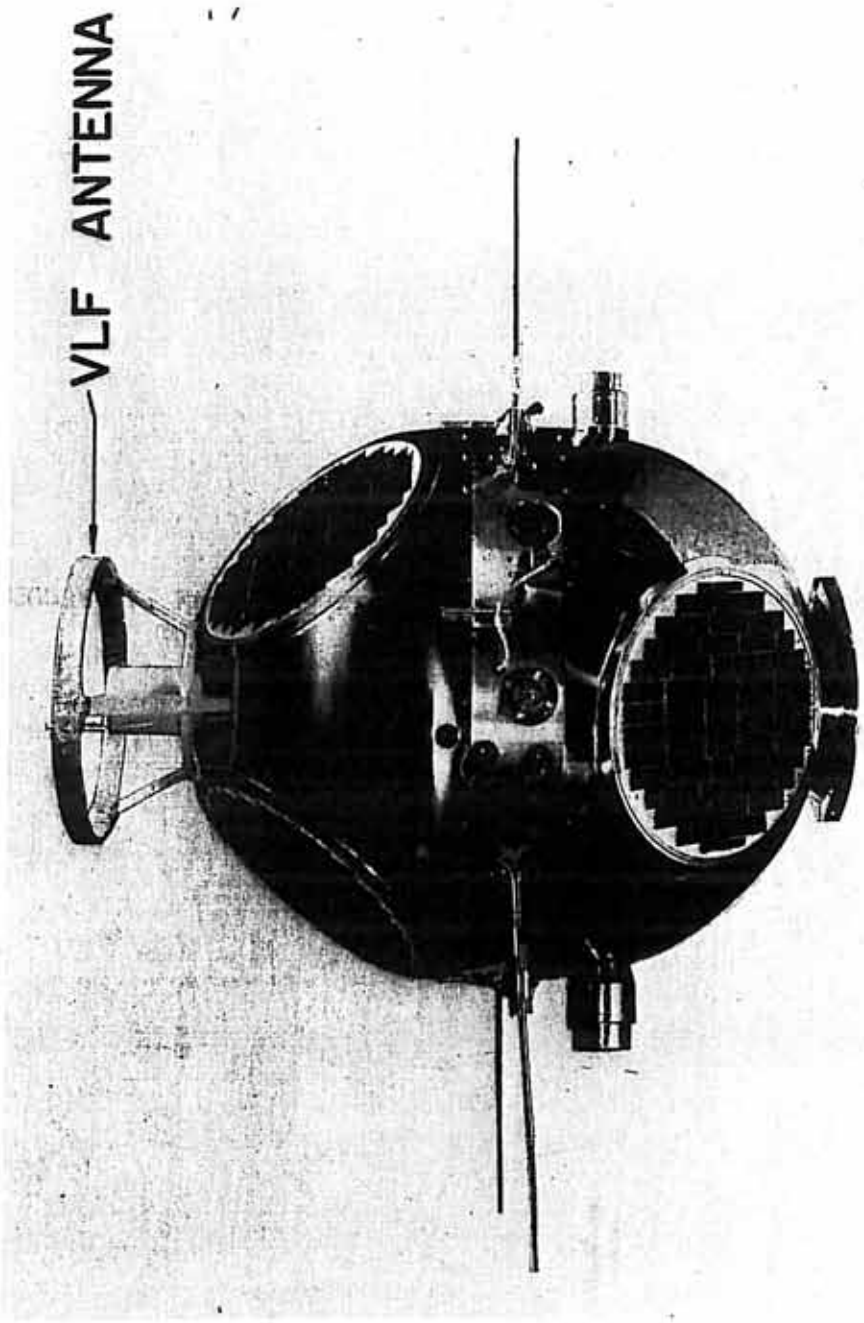

FIGURE 2

FIGURE 3. Frequency response of the Injun 3 wide-band VLF system.

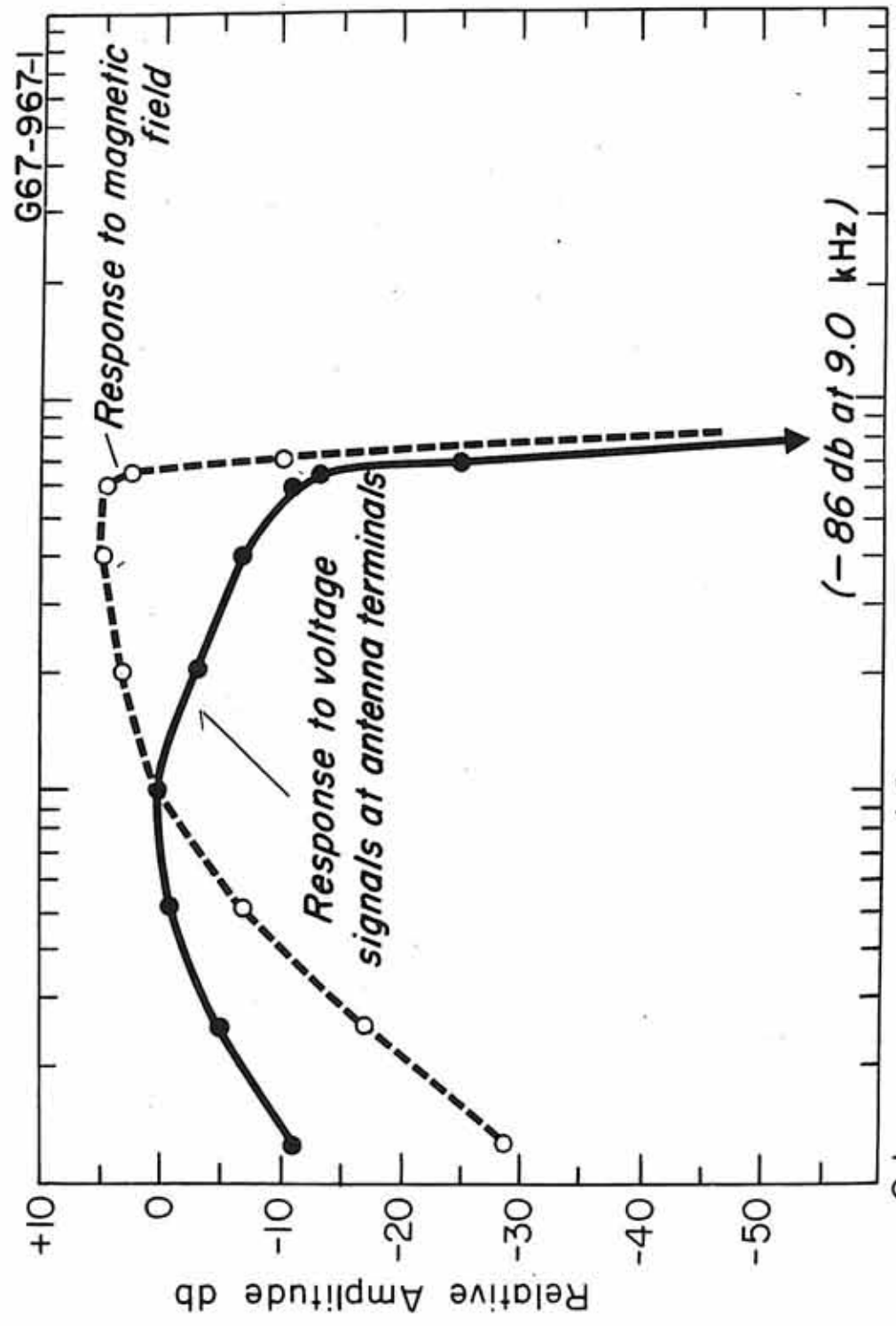
G67-967-1
Response to magnetic field
Response to voltage signals at antenna terminals
(-86 db at 9.0 kHz)
+10
0
-10
-20
-30
-40
-50
Relative Amplitude db
0.1
1.0
10.0
Frequency kHz

FIGURE 3

FIGURE 4. Wide-band VLF field strength, VLF emission spectra, and ≥ 40 keV trapped and precipitated electron fluxes observed by Injun 3 on 7 June 1963. A large magnetic storm began on 6 June.

INJUN 3 REVOLUTION 2196 STATION 13

VLF NOISE SPECTRUM AND INTENSITY

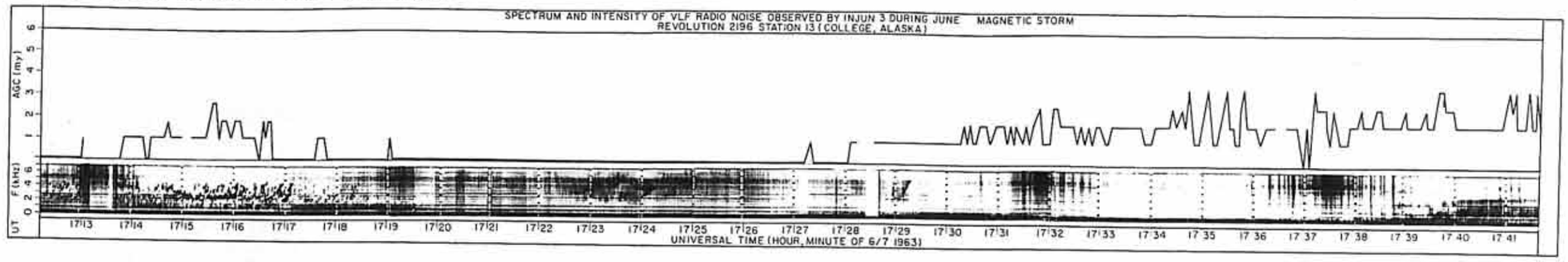

PARTICLE FLUXES AND ORBIT PARAMETERS

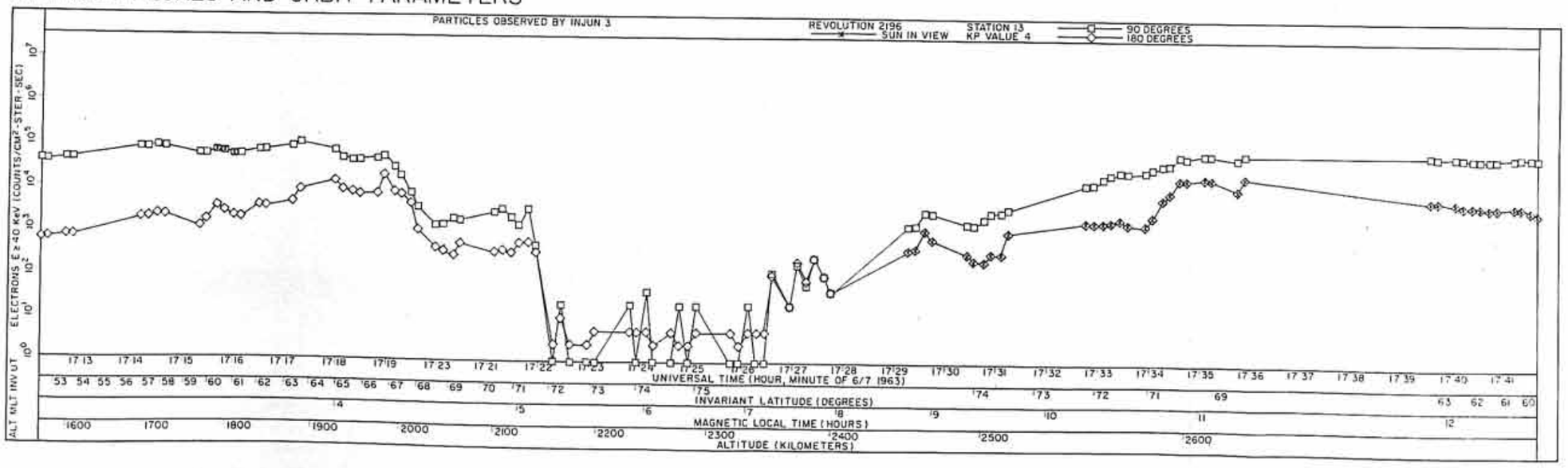

FIGURE 4

FIGURE 5. Wide-band VLF field strength, VLF emission spectra, and ≥ 40 keV trapped and precipitated electron fluxes observed by Injun 3 in magnetic evening on 5 April 1963. A magnetic storm began on 4 April.

G 68-469

INJUN 3 REVOLUTION 1403 STATION 13

VLF NOISE SPECTRUM AND INTENSITY

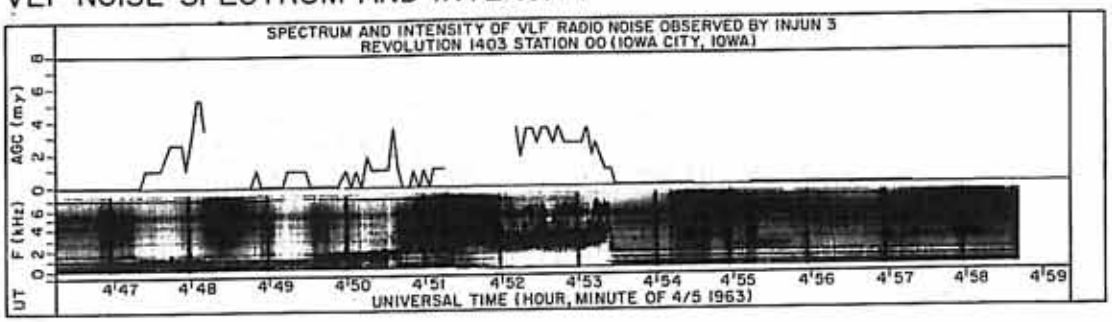

PARTICLE FLUXES AND ORBIT PARAMETERS

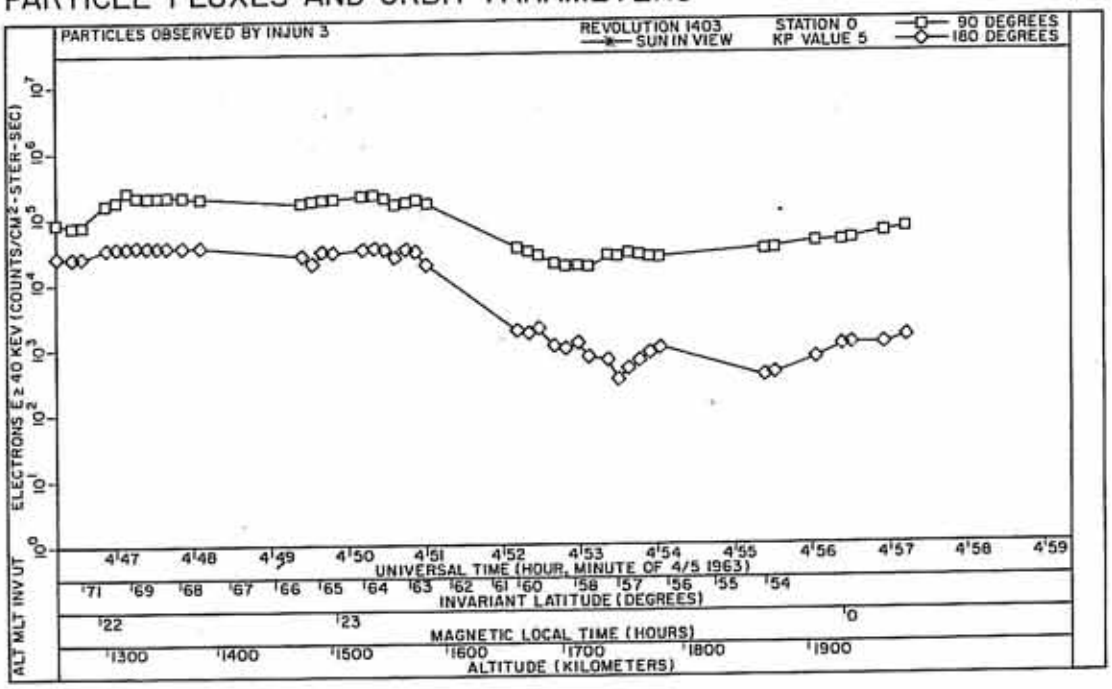

FIGURE 5

FIGURE 6. Orbit of Injun 3 during revolution 2196 while data shown in Figure 4 was being received by the College, Alaska tracking station.

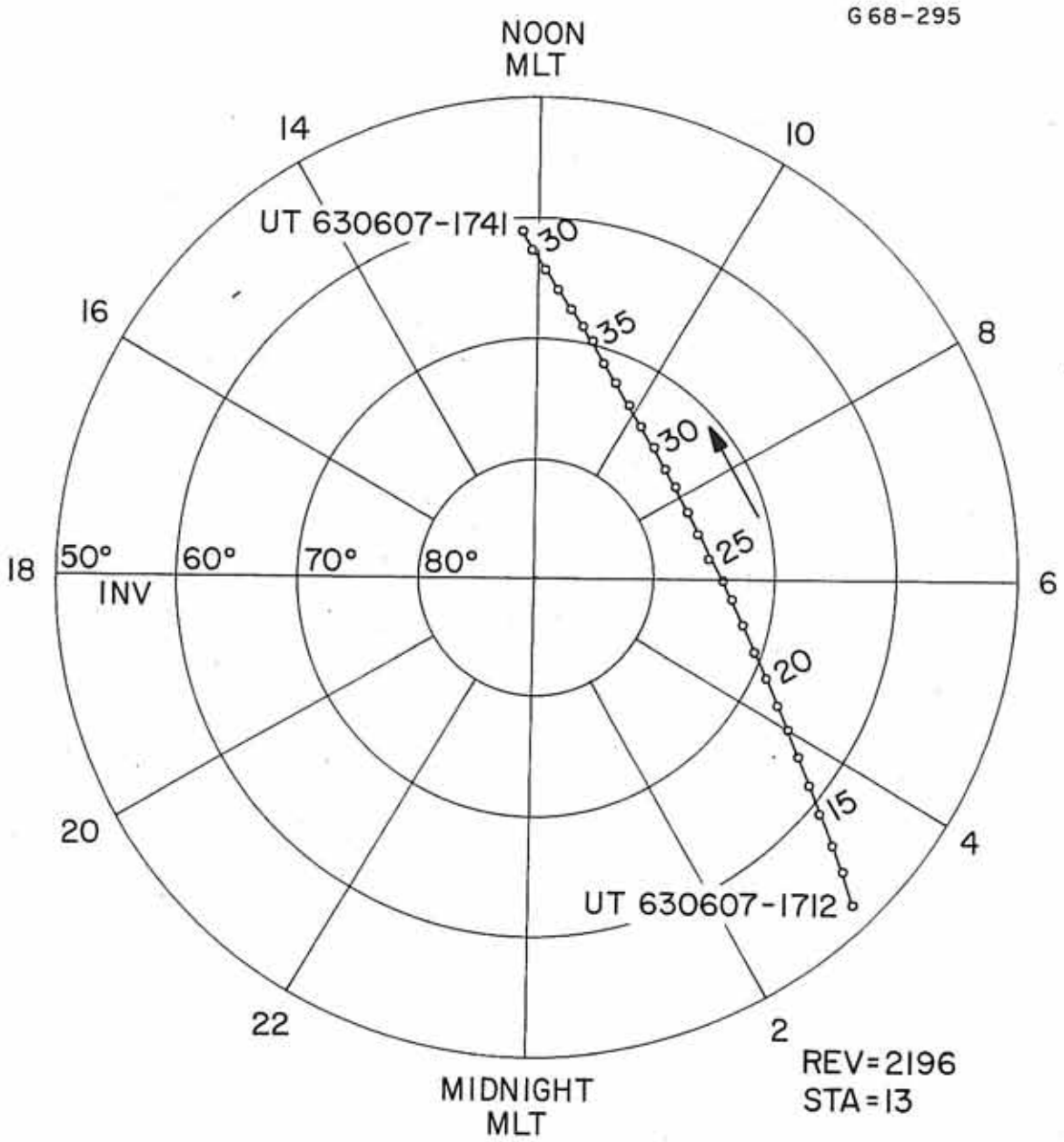
G 68-295
NOON
MLT
14
10
16
8
18
6
20
4
22
2
MIDNIGHT
MLT
50°
60°
70°
80°
INV
UT 630607-1741
UT 630607-1712
30
35
30
25
20
15
REV=2196
STA=13

FIGURE 6

FIGURE 7. Orbit of Injun 3 during revolution 1403 while data shown in Figure 5 was being received by the Iowa City, Iowa tracking station.

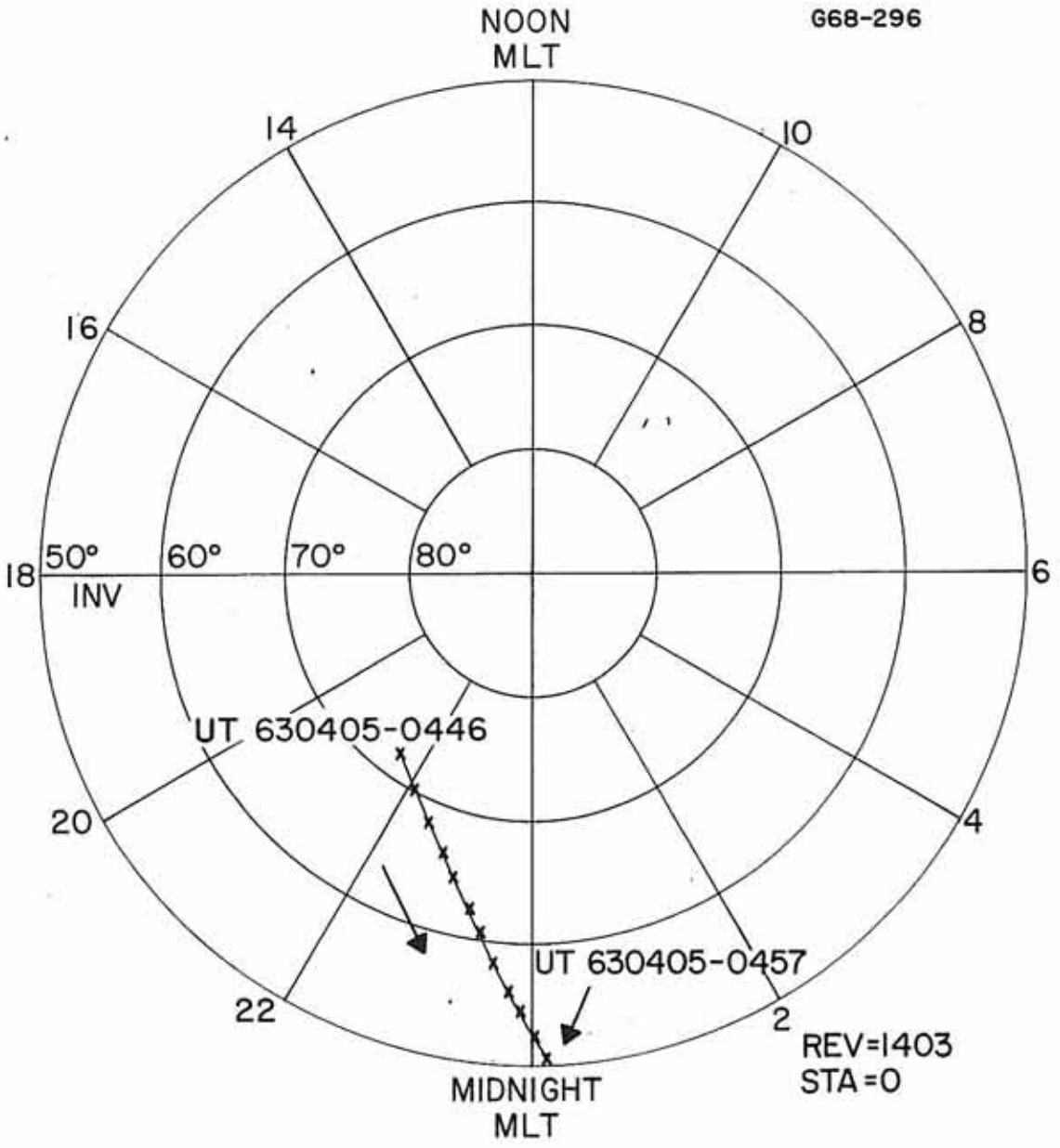
NOON
MLT
G68-296
14
10
16
8
18
50°
INV
60°
70°
80°
6
UT 630405-0446
20
4
UT 630405-0457
22
2
REV=1403
STA=0
MIDNIGHT
MLT

FIGURE 7

FIGURE 8. Sample of VLF emissions observed by Injun 3 in MLT-INV sector 9-60 during the 30 April 1963 magnetic storm. (SC) indicates the sudden commencement of the storm.

G68-462

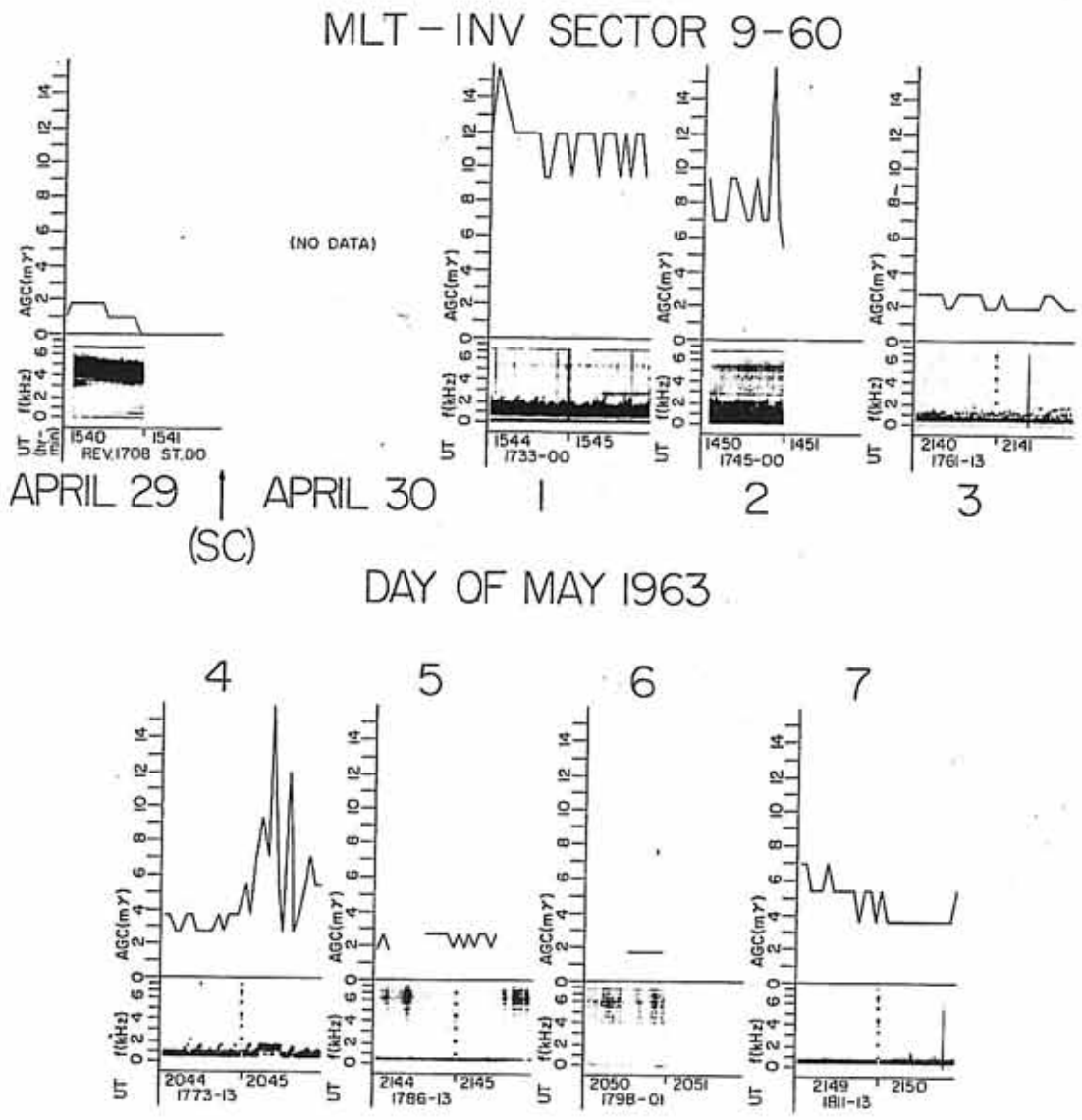

FIGURE 8

FIGURE 9. Sample of VLF emissions observed by Injun 3 in MLT-INV sector 3-50 during the 6 June 1963 magnetic storm. (SC) indicates the sudden commencement of the storm.

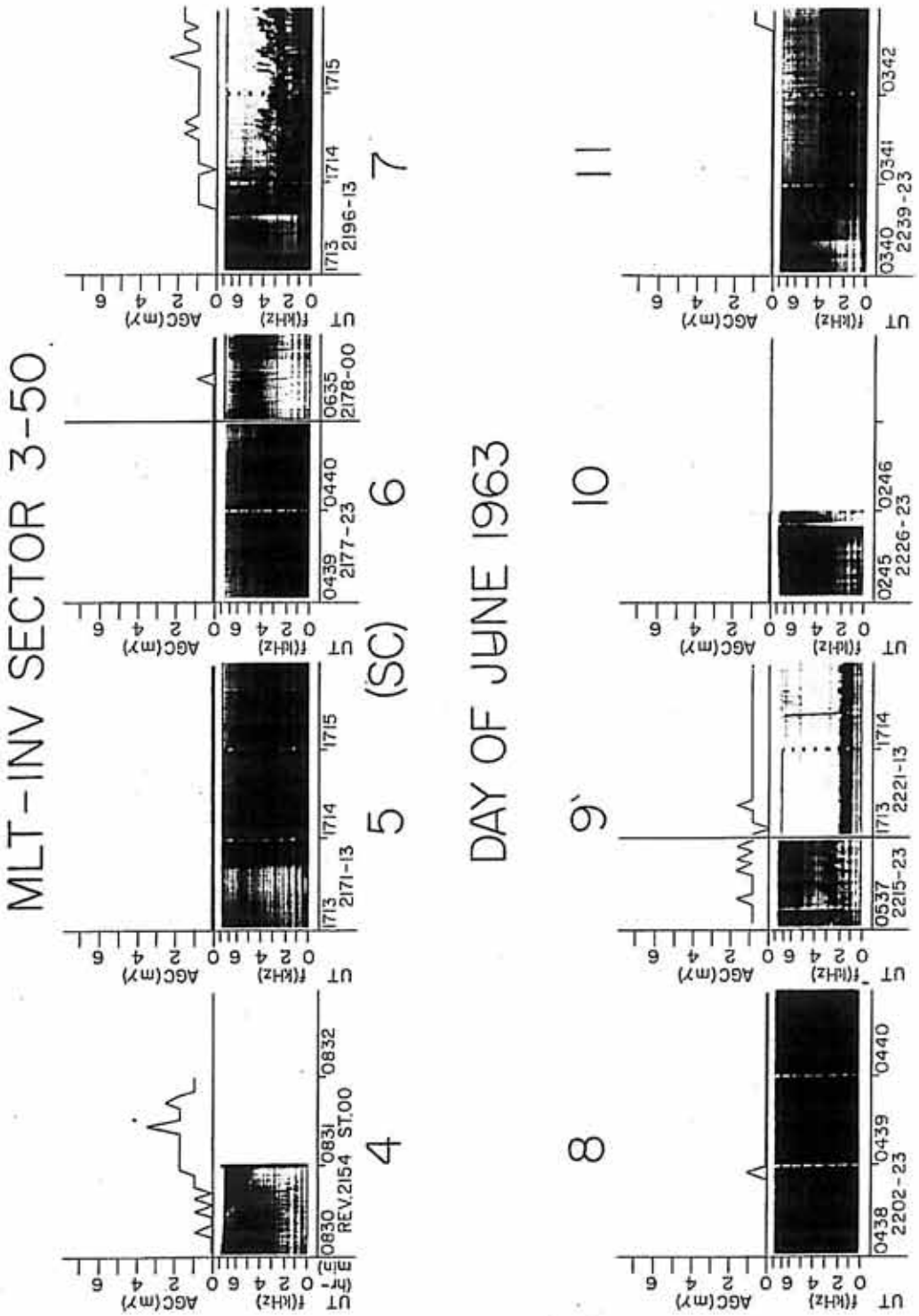
G68-460
MLT-INV SECTOR 3-50
DAY OF JUNE 1963
(SC)
4
5
6
7
8
9'
10
11
UT
f(kHz)
AGC(mγ)
0830
0831
0832
REV.2154 ST.00
1713
1714
1715
2171-13
0439
0440
2177-23
0635
2178-00
2196-13
0438
2202-23
0537
2215-23
2221-13
0245
0246
2226-23
0340
0341
0342
2239-23

FIGURE 9

FIGURE 10. Sample of VLF emissions observed by Injun 3 in MLT-INV sector 5-60 during the 6 June 1963 magnetic storm. (SC) indicates the sudden commencement of the storm.

G68-461

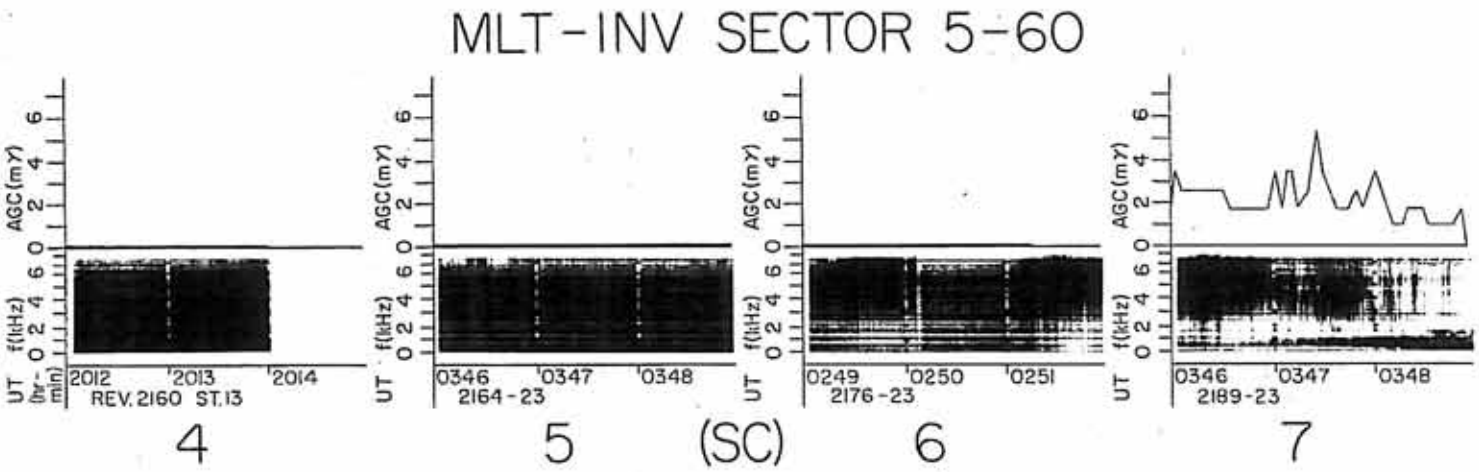

FIGURE 10

FIGURE 11. Sample of VLF emissions observed by Injun 3 in MLT-INV sector 13-50 during the 18 August 1963 magnetic storm. (SC) indicates the sudden commencement of the storm.

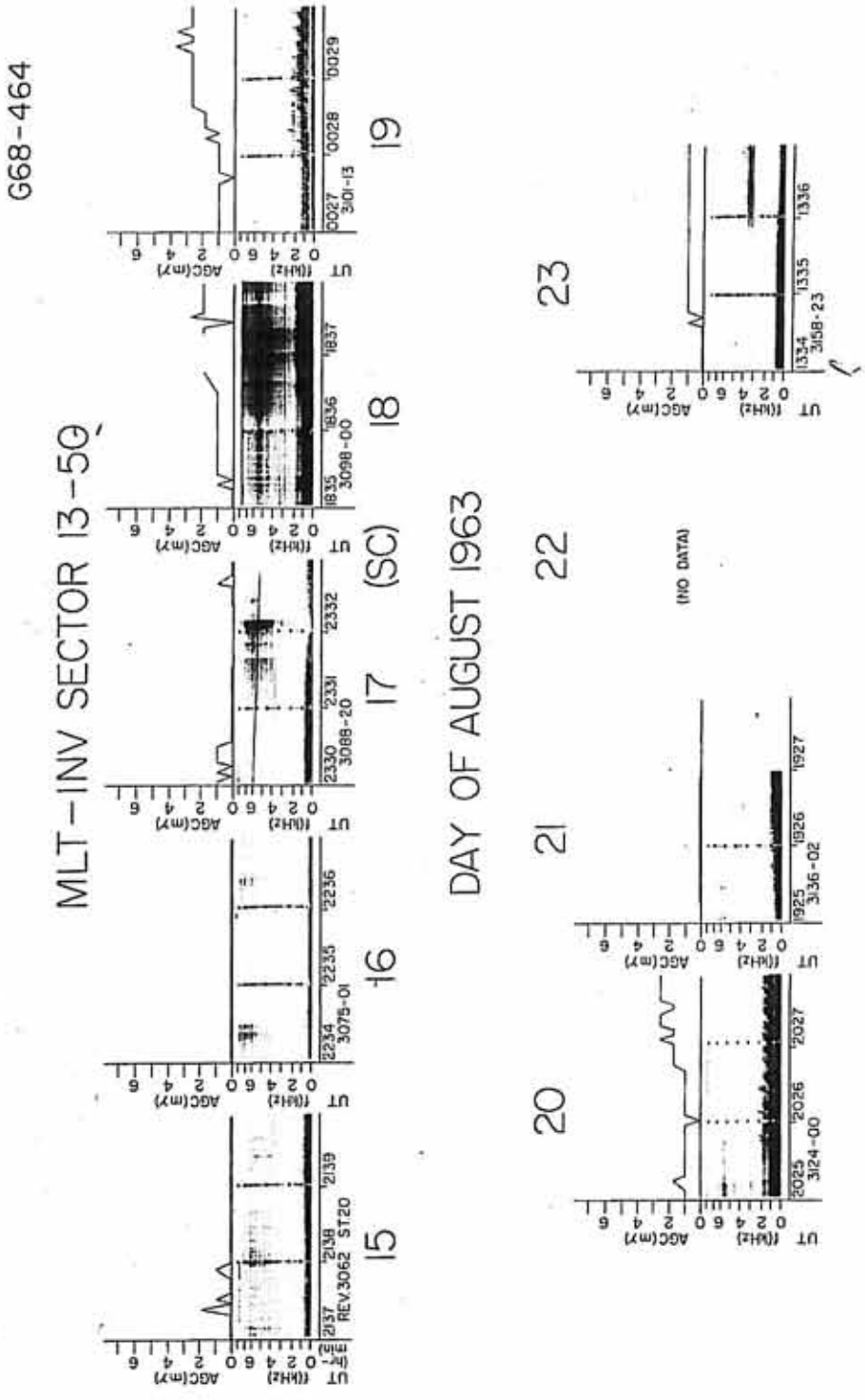
G68-464
MLT-INV SECTOR 13-50
DAY OF AUGUST 1963
(SC)
(NO DATA)
15
16
17
18
19
20
21
22
23

FIGURE 11

FIGURE 12. Sample of VLF emissions observed by Injun 3 in MLT-INV sector 14-60 during the 18 August 1963 magnetic storm. (SC) indicates the sudden commencement of the storm.

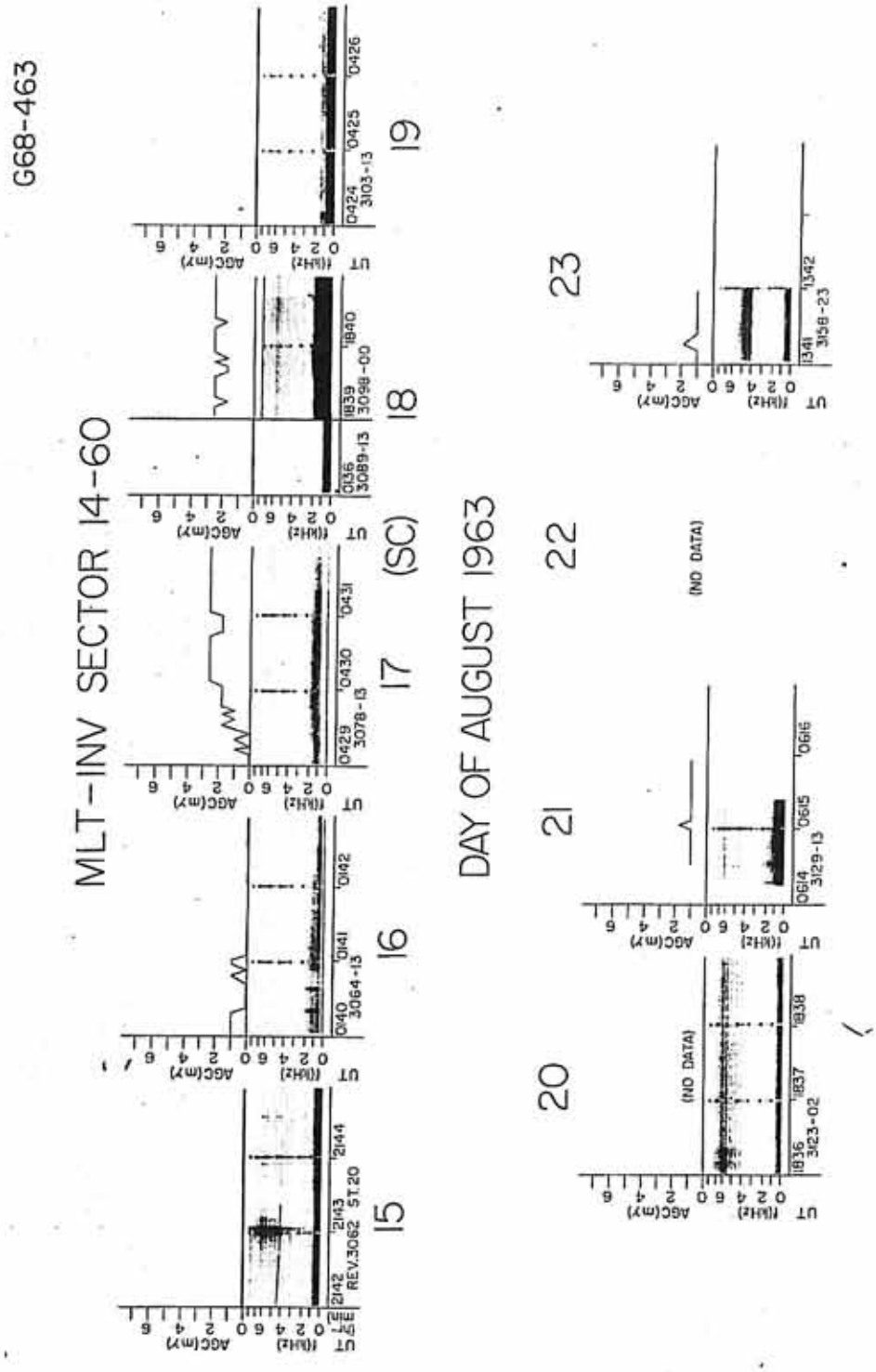
G68-463
MLT-INV SECTOR 14-60
DAY OF AUGUST 1963
15
16
17 (SC)
18
19
20
21
22
23
(NO DATA)
(NO DATA)
UT
f(kHz)
AGC(mγ)
REV.3062 ST.20
3064-13
3078-13
3089-13
3098-00
3103-13
3129-13
3123-02
3358-23

FIGURE 12

FIGURE 13. Time development of chorus during three magnetic storms.

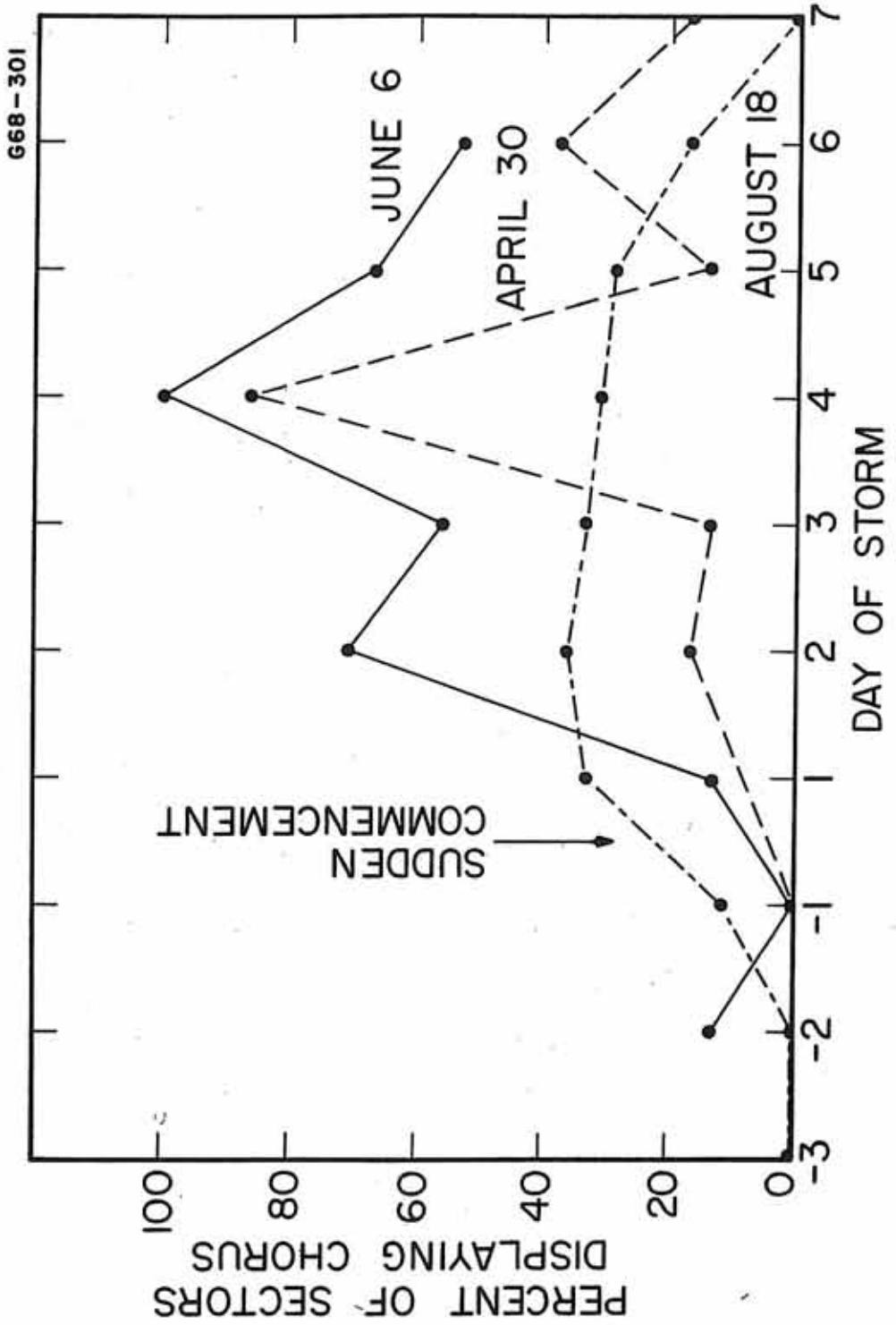
668-301
JUNE 6
APRIL 30
AUGUST 18
SUDDEN COMMENCEMENT
PERCENT OF SECTORS DISPLAYING CHORUS
DAY OF STORM
0
20
40
60
80
100
-3
-2
-1
1
2
3
4
5
6
7

FIGURE 13

FIGURE 14. Time development of ELF hiss, VLF hiss, and chorus during five magnetic storms.

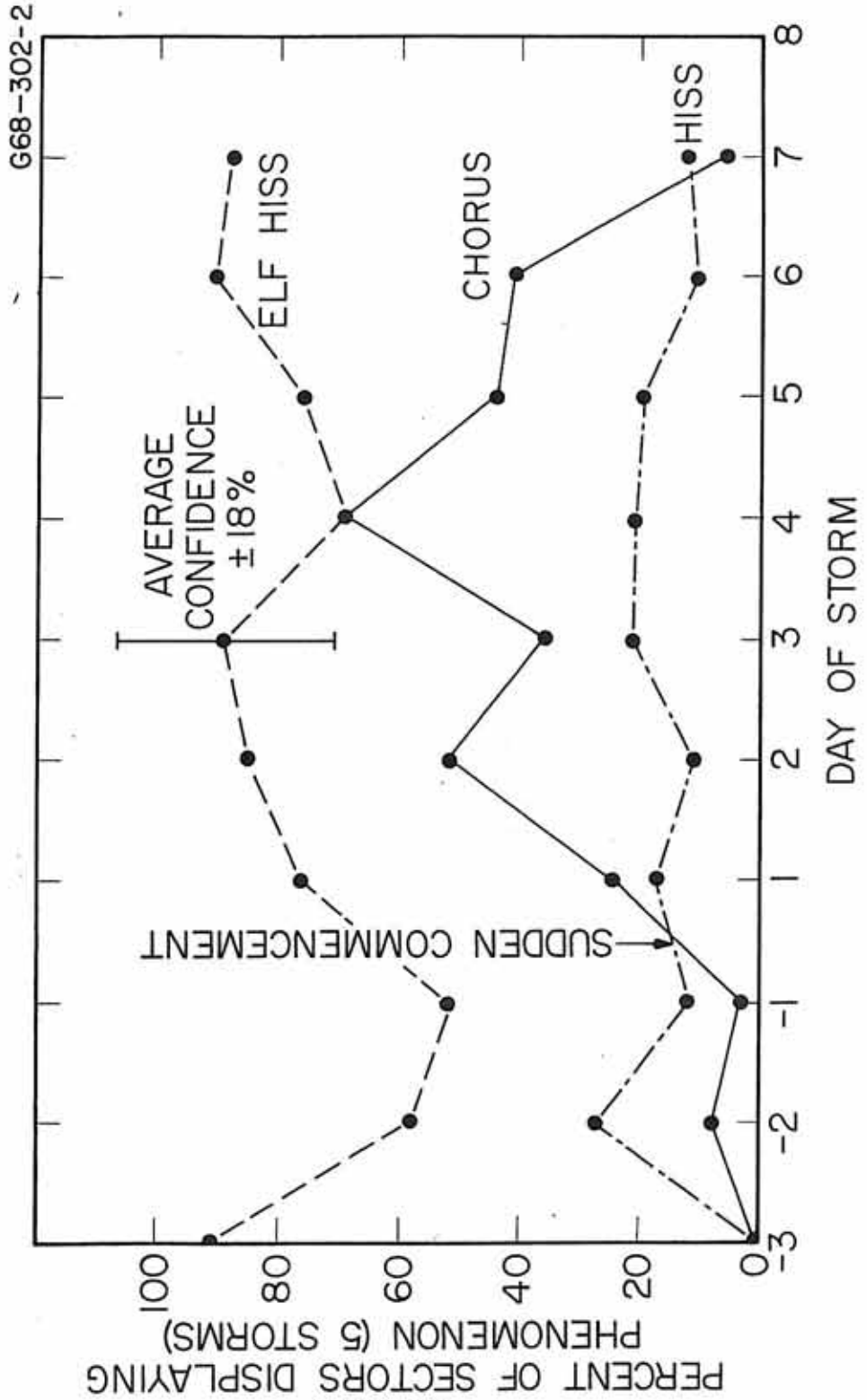
G68-302-2
HISS
CHORUS
ELF HISS
AVERAGE CONFIDENCE ±18%
SUDDEN COMMENCEMENT
PERCENT OF SECTORS DISPLAYING PHENOMENON (5 STORMS)
DAY OF STORM
100
80
60
40
20
0
-3
-2
-1
1
2
3
4
5
6
7
8

FIGURE 14

FIGURE 15. Time-averaged occurrence of chorus in invariant latitude and magnetic local time during five magnetic storm periods. Suggested boundaries of chorus regions are indicated.

G68-300-1

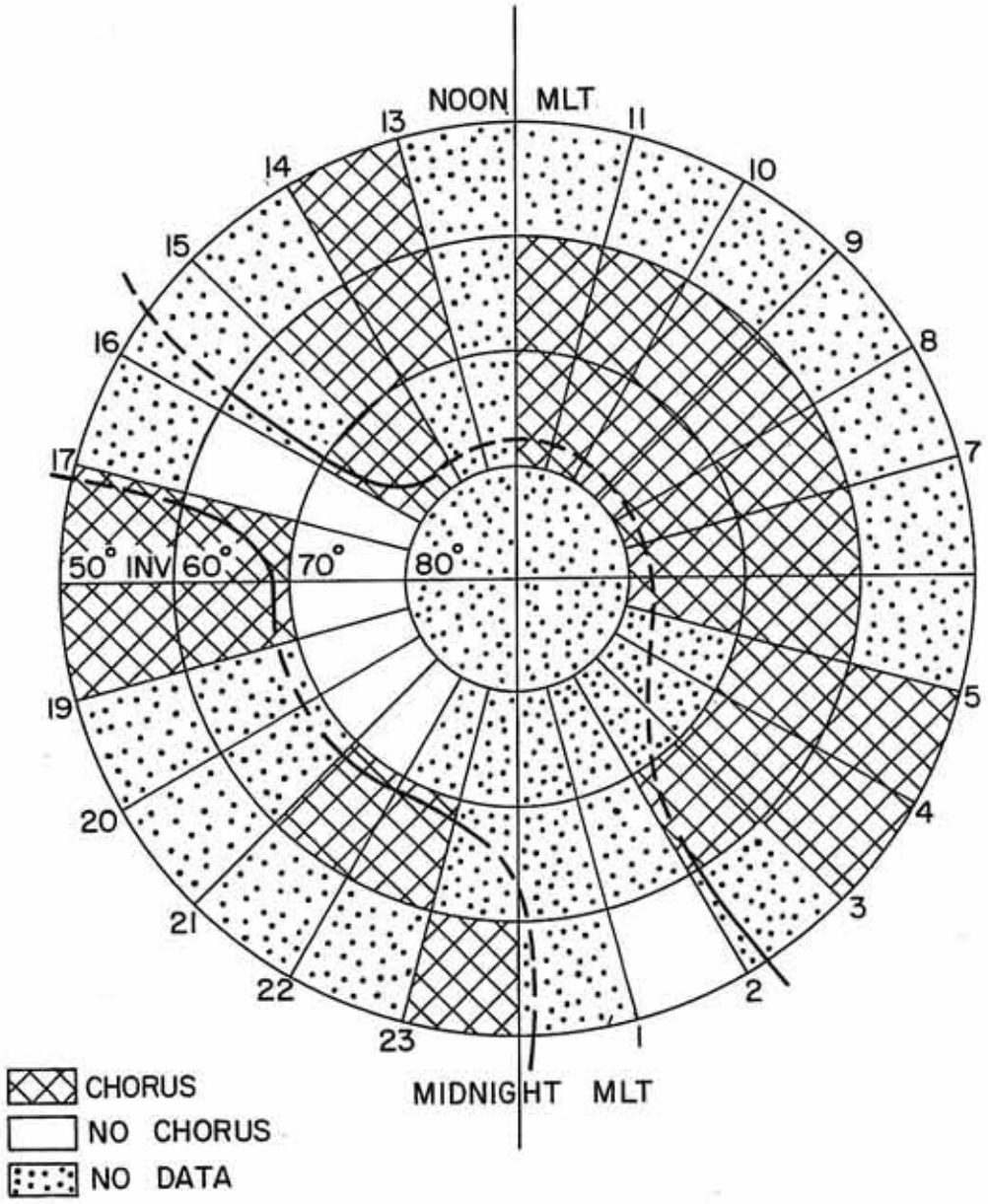

FIGURE 15

FIGURE 16. Daily occurrence of chorus in invariant latitude and magnetic local time during five magnetic storms. Suggested boundaries of chorus regions are indicated.

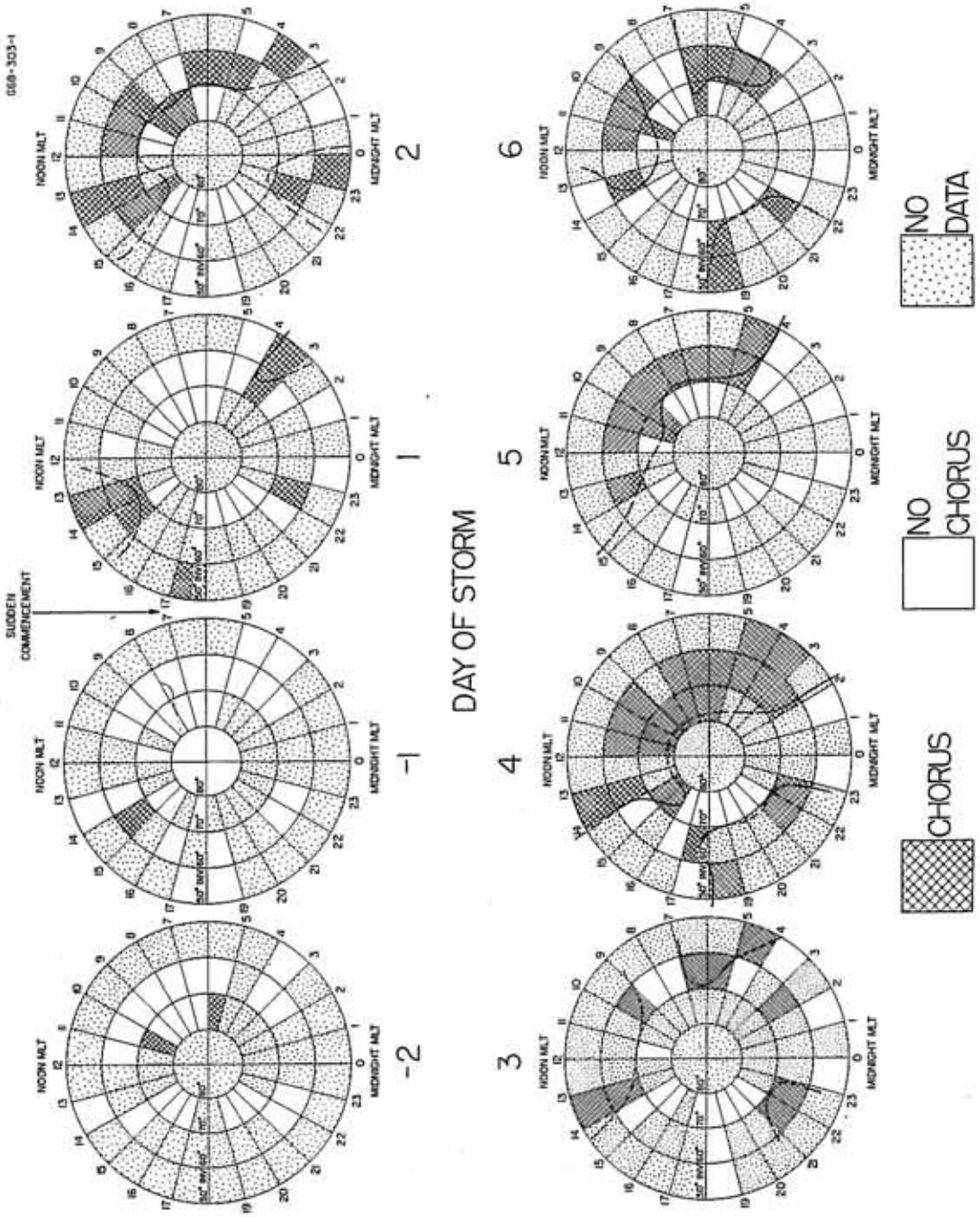
SUDDEN COMMENCEMENT
DAY OF STORM
-2
-1
1
2
3
4
5
6
NOON MLT
MIDNIGHT MLT
CHORUS
NO CHORUS
NO DATA

FIGURE 16

FIGURE 17. Density of data sample used in sector analysis.

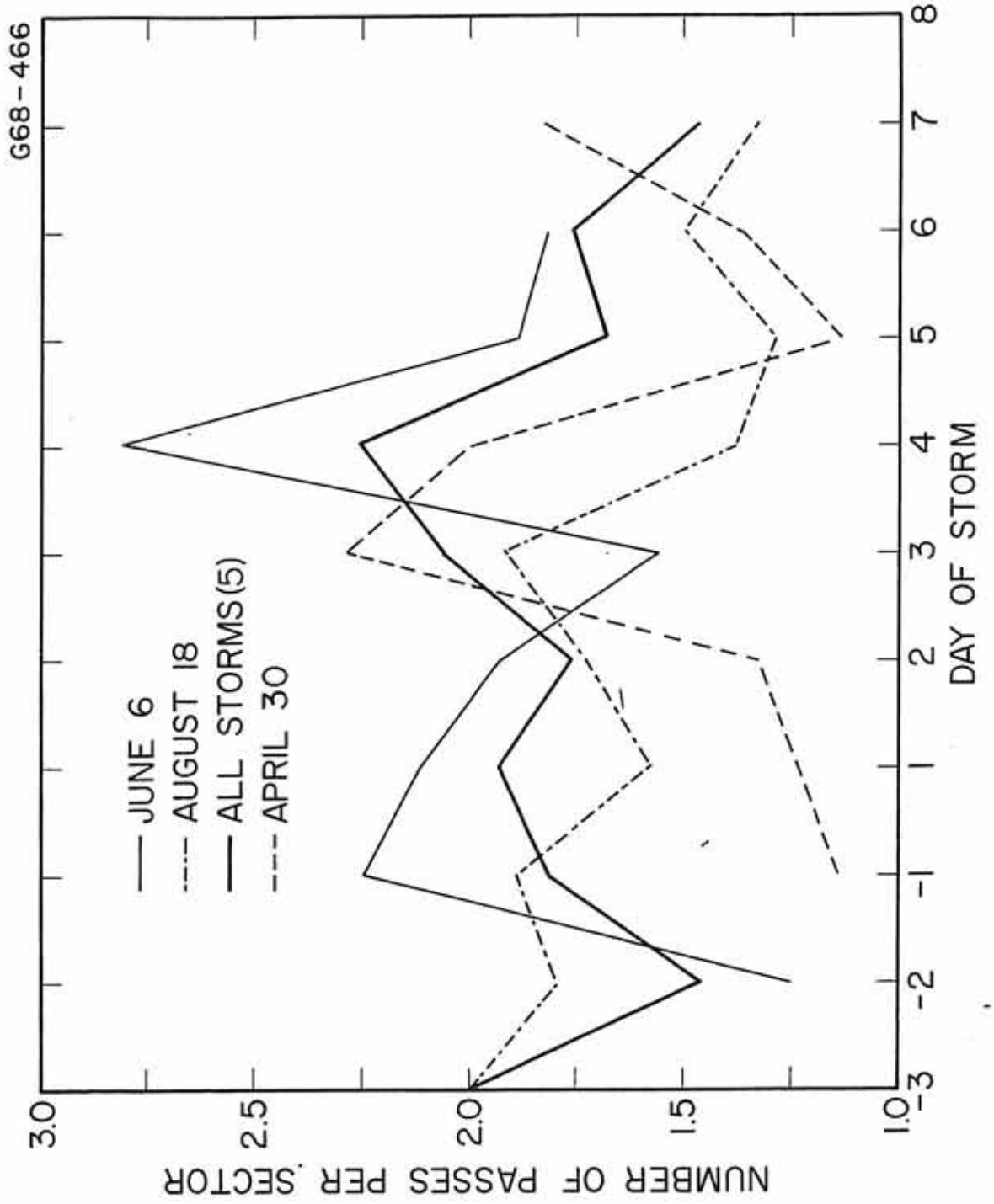
G68-466
JUNE 6
AUGUST 18
ALL STORMS(5)
APRIL 30
NUMBER OF PASSES PER SECTOR
3.0
2.5
2.0
1.5
1.0
-3
-2
-1
1
2
3
4
5
6
7
8
DAY OF STORM

FIGURE 17

FIGURE 18. Injun 3 wide-band VLF field strength contours for May and June, 1963 shown with D_{st} and K_p indices.

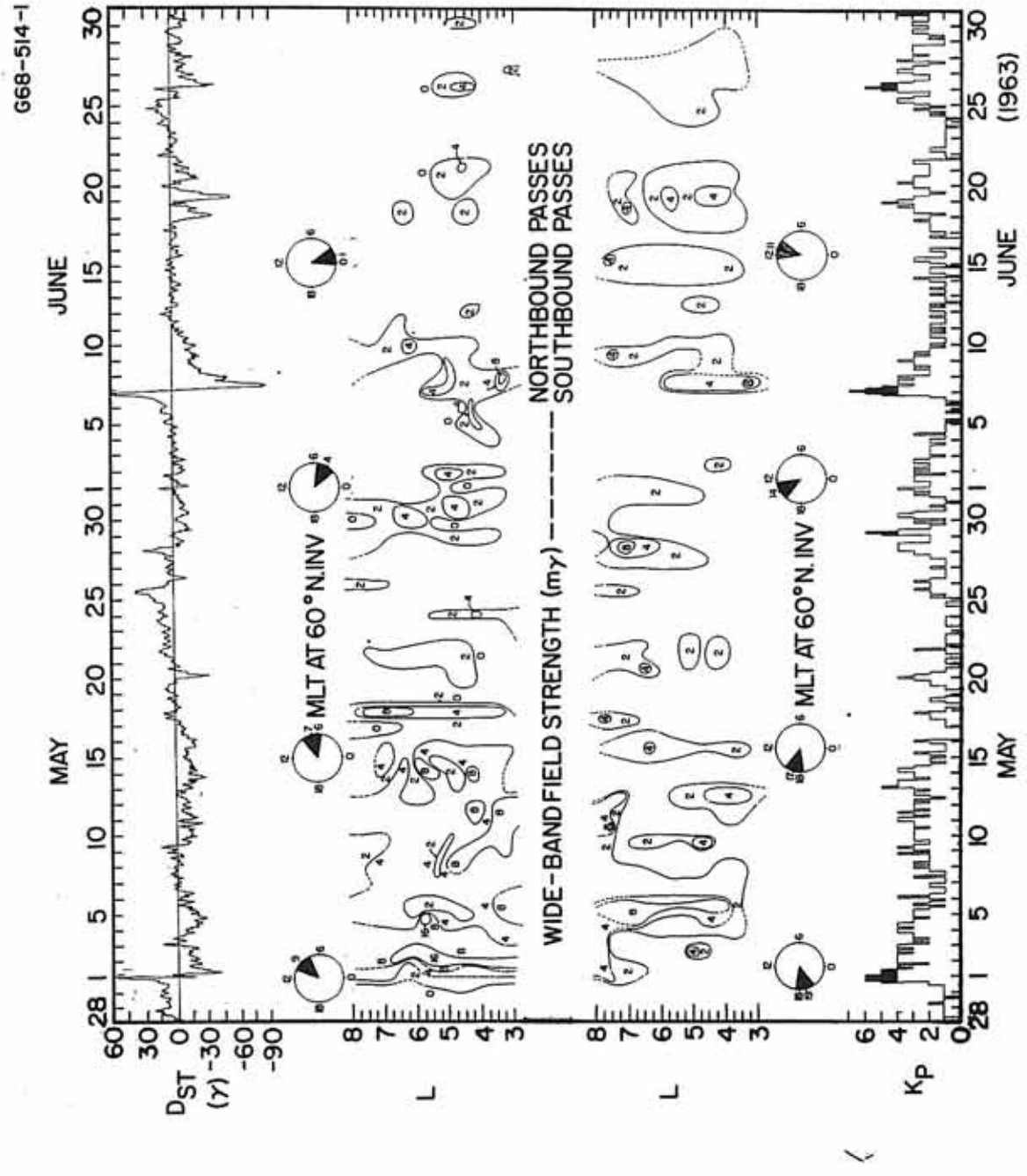
G68-514-1
MAY
JUNE
JUNE
(1963)
MAY
D_{ST} (γ)
L
L
K_P
MLT AT 60° N.INV
MLT AT 60° N. INV
WIDE-BAND FIELD STRENGTH (mγ)
NORTHBOUND PASSES
SOUTHBOUND PASSES

FIGURE 18

FIGURE 19. Continuation of Figure 18 for July and August, 1963.

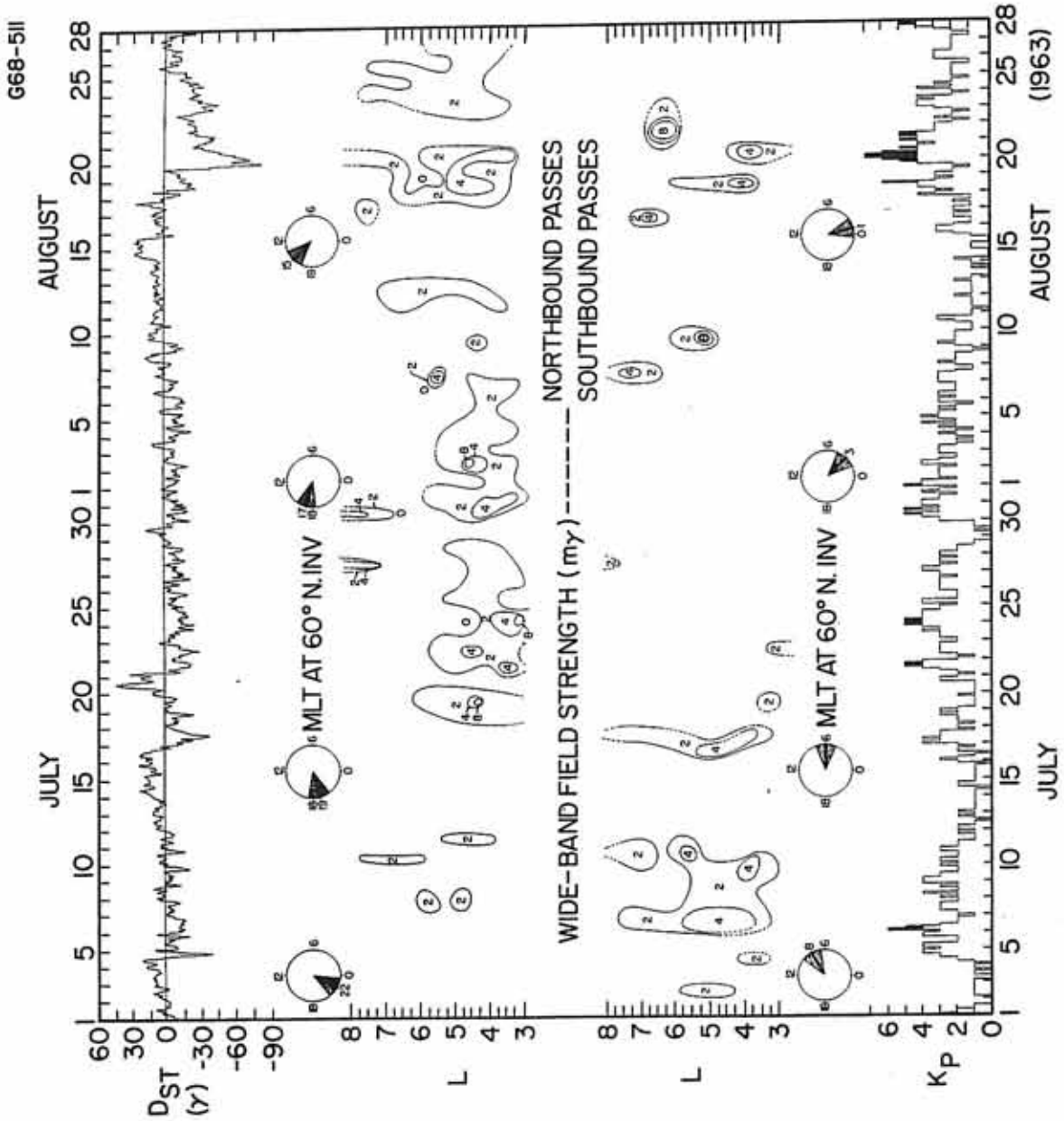
G68-511
JULY
AUGUST
(1963)
D_{ST} (γ)
L
K_P
MLT AT 60° N. INV
WIDE-BAND FIELD STRENGTH (mγ)
NORTHBOUND PASSES
SOUTHBOUND PASSES

FIGURE 19

FIGURE 20. The frequency of occurrence of VLF emissions with wide-band field strengths greater than 1.8 mγ in magnetic local time and invariant latitude (after Taylor and Gurnett [1968]).

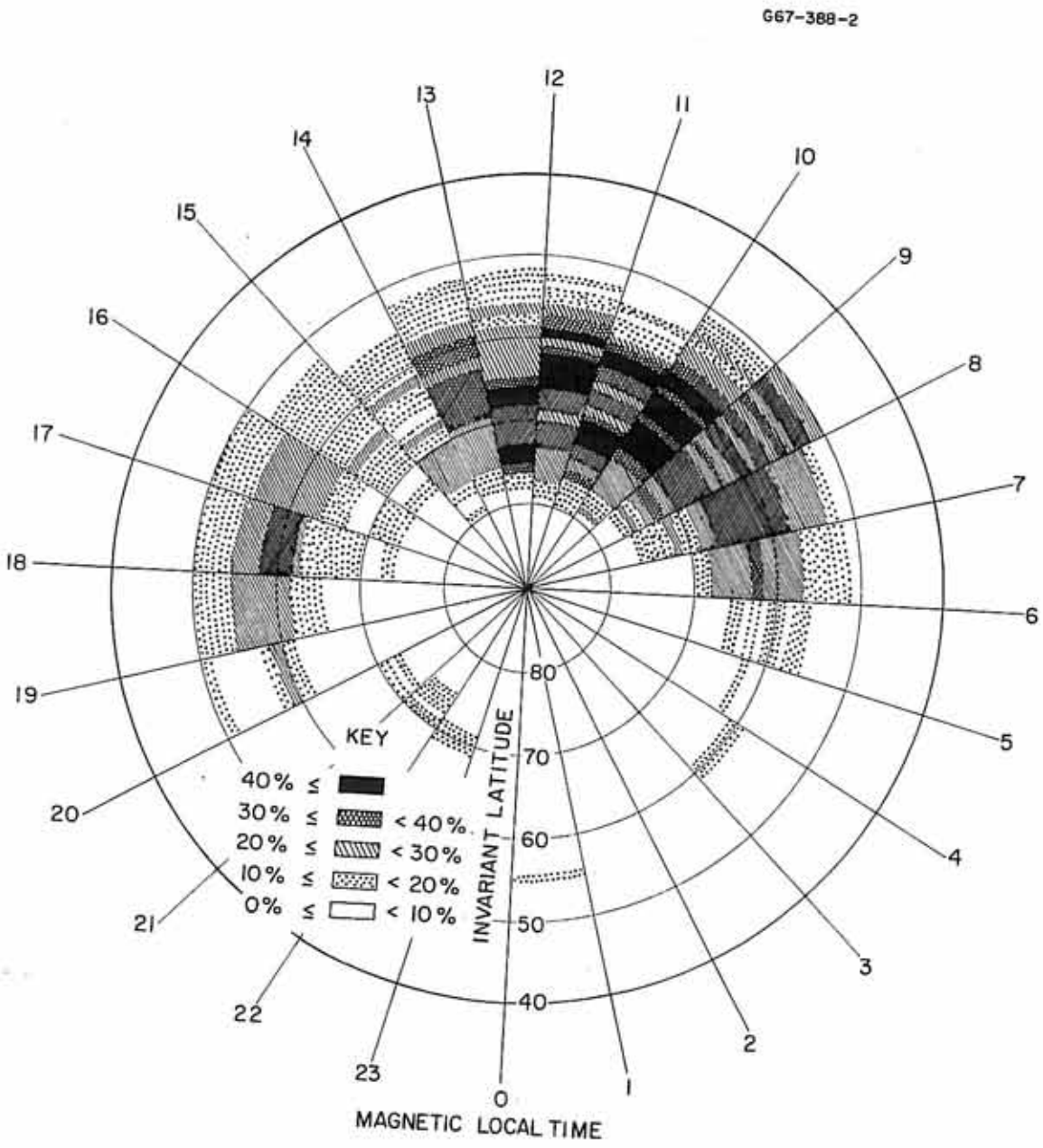
G67-388-2
12
11
10
9
8
7
6
5
4
3
2
1
0
23
22
21
20
19
18
17
16
15
14
13
80
70
60
50
40
INVARIANT LATITUDE
KEY
40% ≤
30% ≤ < 40%
20% ≤ < 30%
10% ≤ < 20%
0% ≤ < 10%
MAGNETIC LOCAL TIME

FIGURE 20

FIGURE 21. Top: Explorer 14 equatorial ≥ 40 keV electron flux contours for June and July, 1963 from Owens and Frank [1968] with regions exceeding the Kennel-Petschek limiting flux indicated.

Bottom: Injun 3 wide-band VLF field strength contours.

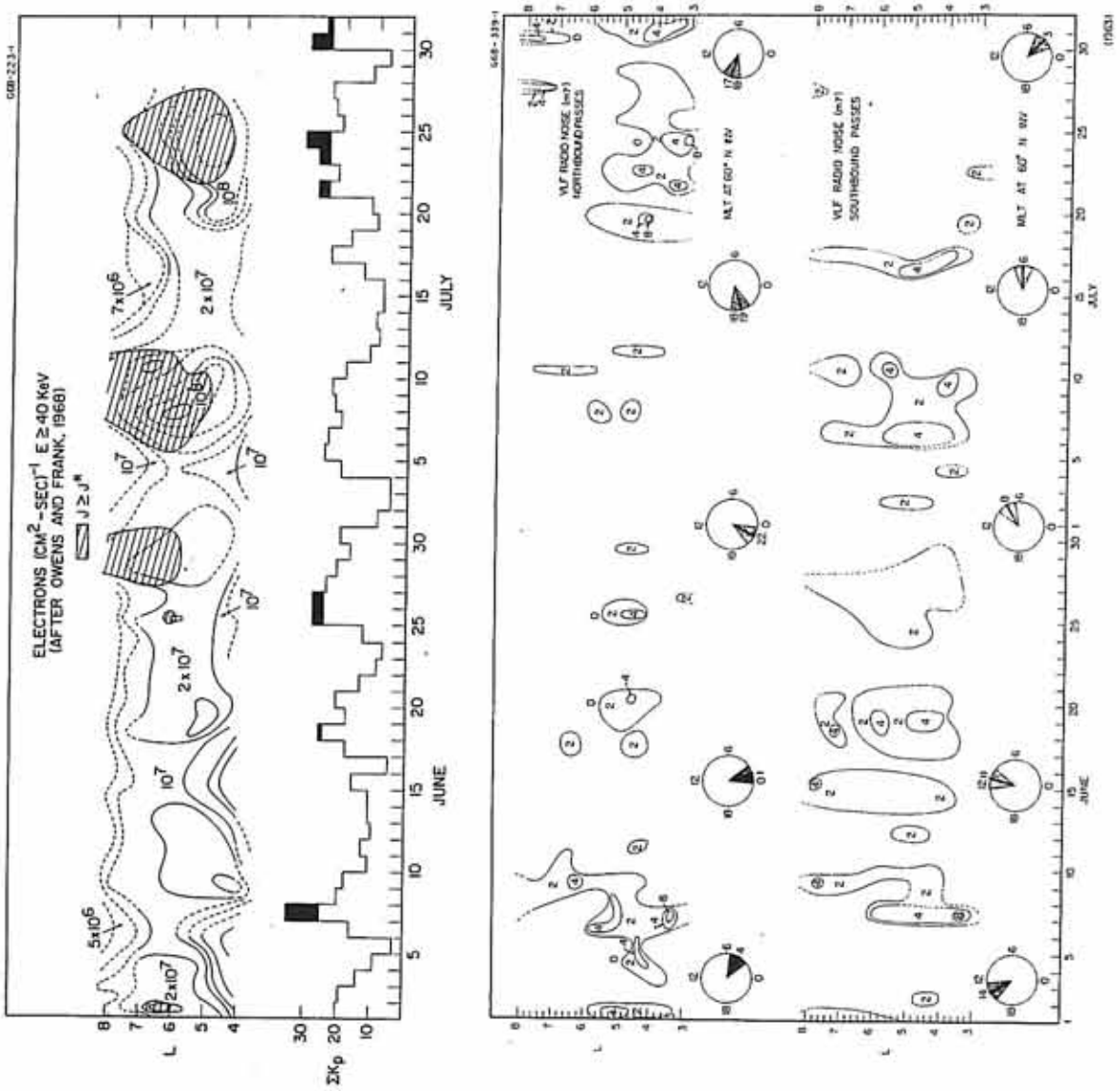
ELECTRONS (CM²-SEC)⁻¹ E ≥ 40 KeV
(AFTER OWENS AND FRANK, 1968)
J ≥ J*
5x10⁶
2x10⁷
10⁷
2x10⁷
7x10⁶
10⁸
2x10⁷
10⁷
10⁷
L
ΣKp
JUNE
JULY
VLF RADIO NOISE (m²)
NORTHBOUND PASSES
VLF RADIO NOISE (m²)
SOUTHBOUND PASSES
MLT AT 60° N LAT
MLT AT 60° N LAT

FIGURE 21